Summer 8-2010

INVESTIGATION INTO CURRENT EFFICIENCY FOR PULSE ELECTROCHEMICAL MACHINING OF NICKEL ALLOY

Yu Zhang
University of Nebraska at Lincoln, zhang.yu@huskers.unl.edu

INVESTIGATION INTO CURRENT EFFICIENCY FOR PULSE ELECTROCHEMICAL MACHINING OF NICKEL ALLOY

By

Yu Zhang

A THESIS

Presented to the Faculty of

The Graduate College at the University of Nebraska

In Partial Fulfillment of Requirements

For the Degree of Master of Science

Major: Industrial and Management Systems Engineering

Under the Supervision of Professor Kamlakar P. Rajurkar

Lincoln, Nebraska

August, 2010

INVESTIGATION INTO CURRENT EFFICIENCY FOR PULSE ELECTROCHEMICAL MACHINING OF NICKEL ALLOY

Yu Zhang, M.S.

University of Nebraska, 2010

Adviser: Kamlakar P. Rajurkar

Electrochemical machining (ECM) is a nontraditional manufacturing process that can machine difficult-to-cut materials. In ECM, material is removed by controlled electrochemical dissolution of an anodic workpiece in an electrochemical cell. ECM has extensive applications in automotive, petroleum, aerospace, textile, medical, and electronics industries.

Improving current efficiency is a challenging task for any electro-physical or electrochemical machining processes. The current efficiency is defined as the ratio of the observed amount of metal dissolved to the theoretical amount predicted from Faraday's law, for the same specified conditions of electrochemical equivalent, current, etc [1]. In macro ECM, electrolyte conductivity greatly influences the current efficiency of the process. Since there is a certain limit to enhance the conductivity of the electrolyte, a process innovation is needed for further improvement in current efficiency in ECM. Pulse electrochemical machining (PECM) is one such approach in which the electrolyte conductivity is improved by electrolyte flushing in pulse off-time.

The aim of this research is to study the influence of major factors on current efficiency in a pulse electrochemical machining process in macro scale and to develop a linear regression model for predicting current efficiency of the process.

An in-house designed electrochemical cell was used for machining nickel alloy (ASTM B435) by PECM. The effects of current density, type of electrolyte, and electrolyte flow rate, on current efficiency under different experimental conditions were studied. Results indicated that current efficiency is dependent on electrolyte, electrolyte flow rate, and current density. Linear regression models of current efficiency were compared with twenty new data points graphically and quantitatively. Models developed were close enough to the actual results to be reliable.

In addition, an attempt has been made in this work to consider those factors in PECM that have not been investigated in earlier works. This was done by simulating the process by using COMSOL software. However, it was found that the results from this attempt were not substantially different from the earlier reported studies.

ACKNOWLEDGEMENTS

I would like to express my sincerest gratitude to Dr. Kamlakar P. Rajurkar for his support and continuous guidance throughout my graduate study and research at the University of Nebraska. His suggestions and commitment have been a great source of inspiration for my research, as well as my personal life.

I also would like to thank my committee members, Dr. Robert Williams and Dr. David Cochran, for their suggestions and contribution.

No thanks are enough for Dr. Murali Sundaram and Dr. Lin Gu. Their guidance and constant help has made the whole project possible.

Special thanks are due to my fellow students in the Center for Nontraditional Manufacturing Research for sharing ideas and knowledge. The supportive spirits and encouragements among us create a positive research atmosphere and also make my stay here comfortable.

I thank the Machine Shop staff for their help with materials, the English Writing Center students for their help with writing, and my friends in Engineering College. The conversations and discussions with them inspired me and opened a wide window to other fields.

Finally, I must thank my parents and grandparents. Their love and support have always been with me.

TABLE OF CONTENTS

LIST OF FIGURES

FIGURE PAGE

LIST OF TABLES

CHAPTER 1

INTRODUCTION

1.1 Electrochemical Machining

Electrochemical machining (ECM) was developed to machine difficult-to-cut materials, and it is an anodic dissolution process based on the phenomenon of electrolysis, whose laws were established by Michael Faraday [1]. In ECM, electrolytes serve as conductors of electricity. ECM offers a number of advantages over other machining methods and also has several disadvantages:

Advantages: there is no tool wear; machining is done at low voltages compared to other processes with high metal removal rate; small dimensions can be controlled; hard conductive materials can be machined into complicated profiles; workpiece structure suffer no thermal damages; suitable for mass production work and low labor requirements.

Disadvantages: a huge amount of energy is consumed that is approximately 100 times that required for the turning or drilling of steel; safety issues on removing and disposing of the explosive hydrogen gas generated during machining; and difficulty in handling and containing the electrolyte [2].

As shown in figure 1.1, the shaped tool (cathode) is connected to the negative polarity and the workpiece (anode) is connected to the positive polarity. The electrolyte flows through the small interelectrode gap, thus flushing away sludge and heat generated during machining process.

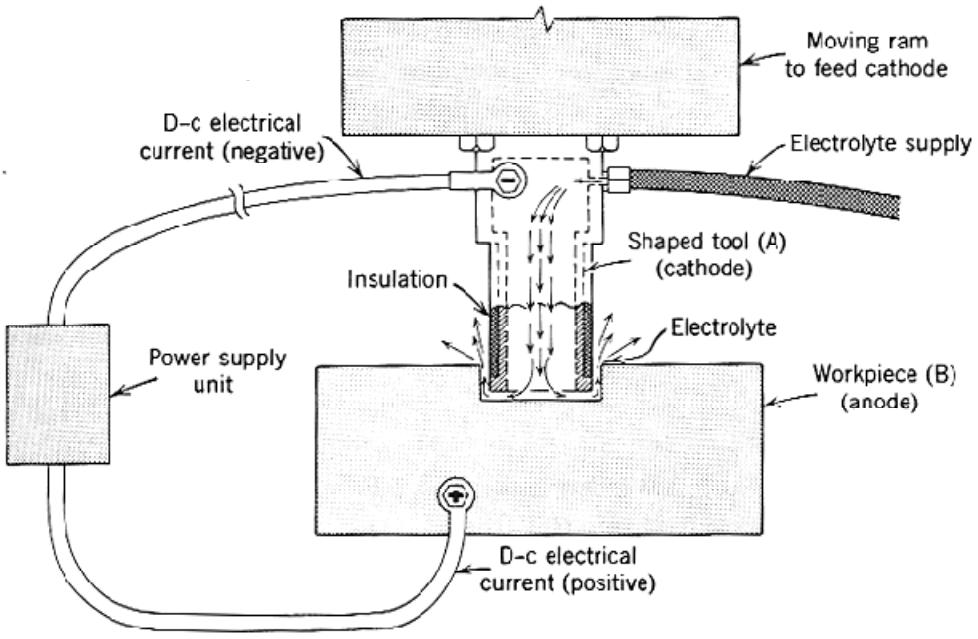

Fig. 1.1 Principle of Electrochemical Machining [3]

1.2 Pulse Electrochemical Machining

Pulse electrochemical machining (PECM) is based on electrochemical principles, mainly the use of pulsed voltage or pulsed current relaxation, to enhance the activity of the cathode reducing the cathode polarization and concentration polarization, thus effectively improve the energy usage of the process [4]. The schematic of PECM system with typical input parameters (blue) is shown in the figure 1.2.

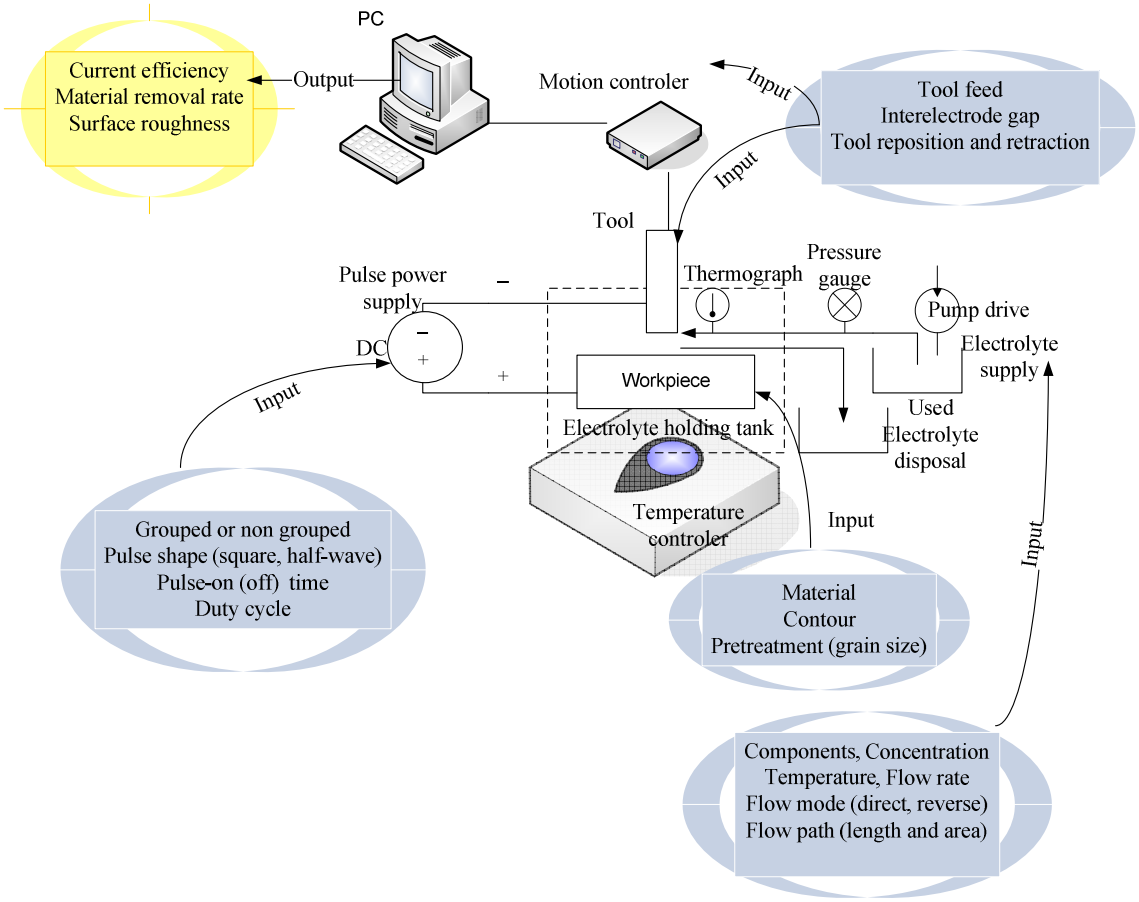

Fig. 1.2 Schematic diagram and related parameters of PECM system

For each of the main components of PECM such as power supply, material geometry, control system, and electrolytes, there are various input factors that can affect the output parameters (yellow) such as current efficiency, material removal rate and surface roughness[5,6]. In PECM, smaller interelectrode gap may be obtained. The development of a high current efficiency is the key to further advancement in PECM. Recent studies show that, as compared with ECM, PECM results in improved anodic dissolution efficiency, more stable interelectrode gap state, and better surface finish [7]. Investigations of the process mechanism and parameter optimization are needed to obtain

a better understanding of the complex interactions of electrical, chemical, and physical parameters in PECM [8]. Table 1.1 indicates the comparison of PECM and ECM.

Table 1.1 Comparison of PECM and ECM [1, 3]

	PECM	ECM
Principle	electrolysis	electrolysis
Power supply	pulse	constant
Current density	10-103 A/cm^2	8-233A/cm^2
Voltage	7-25V	4-30V
Electrolyte velocity	10-60 m/sec	15-60 m/sec
Gap	Less than 0.10mm	0.025-0.76mm
Surface quality	Improved than ECM	
Metal removal rate	Lower than ECM	
Cost	More expensive than ECM	

1.3 Fundamental Principles

Ions and electrons crossing phase boundaries (the interface between two or more separate phases, such as liquid-solid) would result in electron transfer reactions carried out at both anode and cathode. Meanwhile, the potential difference is fundamental in understanding the energy distribution during the electrochemical machining process. Figure 1.3 shows the broad concepts and basic potential calculation methods. Nernst equation is used to calculate the electrode reversible potential. Tafel equation, diffusion layer, and ohm's law can assist in estimating activation overpotential, concentration

overpotential, and resistance overpotential, which are known as the three main overpotentials in electrochemical reactions.

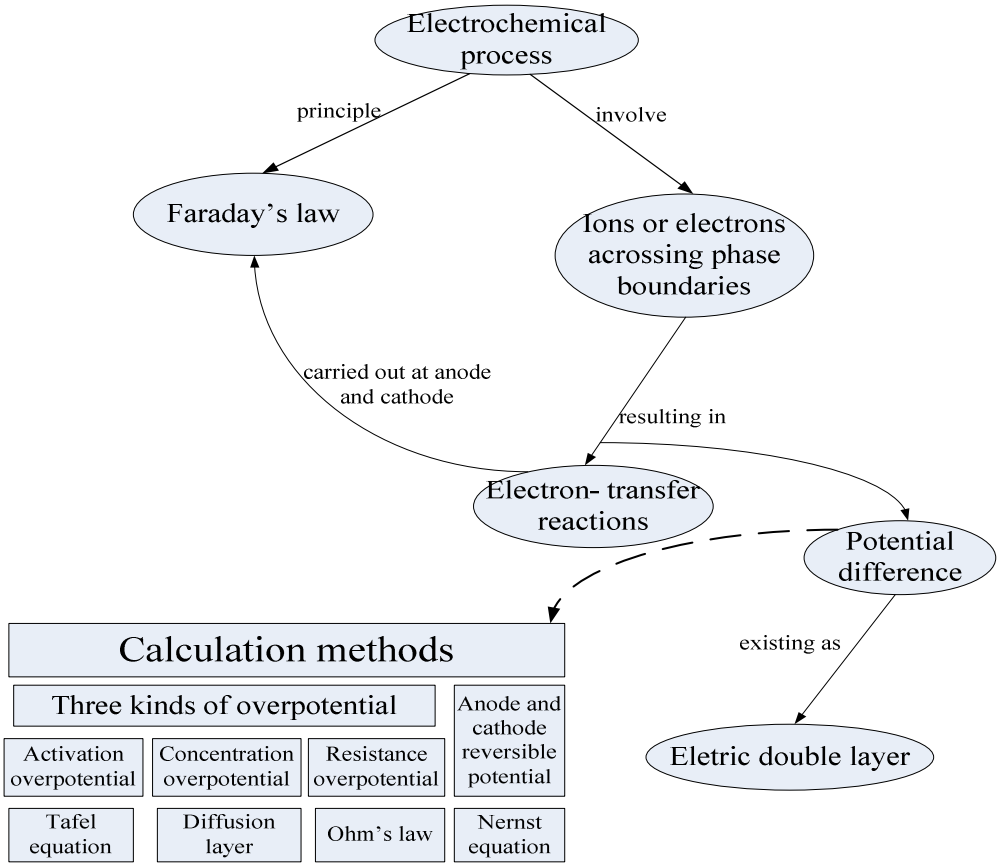

Fig. 1.3 Overall concepts and calculation methods for potentials

1.4 Research Objectives

The goal of this thesis was to investigate current efficiency in pulse electrochemical machining of nickel alloy. The objectives of this thesis are to:

1. conduct an experimental study to identify the factors influencing the current efficiency of pulse electrochemical machining.

2. establish quantitative relationship between process parameters and current efficiency.
3. build a simulation model to explain the effect of the process parameters on current efficiency and to understand the mechanism of pulse electrochemical machining.

1.5 Thesis Organization

Chapter two consists of a literature review describing the metal dissolution process, valence state estimation, anode potential, types of electrolytes, pulse parameters, nickel alloy machining methods, current efficiency definition and the factors influencing current efficiency.

Chapter three presents the experimental setup and design, experimental results, and statistical analysis.

Chapter four describes the simulation process for the anodic dissolution process of PECM.

Chapter five makes the conclusions and offers recommendations into future research.

CHAPTER 2

LITERATURE REVIEW

2.1 Introduction

The metal dissolution process, valence state estimation, anode potential, types of electrolyte, pulse parameters, nickel alloy machining methods, current efficiency definition and influencing factors are discussed and summarized in this chapter.

2.2 Metal Dissolution Process

Since electrolysis is the main part of ECM, it must be understood before going further through the characteristics and other details of the process. Atom-by-atom removal of metal by anodic dissolution is the basic principle underlying electrochemical metal removal process. The movement of the ions is accompanied by electrons flow, in the opposite direction to the positive current in the electrolyte.

The reactions are a consequence of the applied potential difference, that is, voltage from the electric source [1, 9]. The phenomena can be embodied in Faraday's laws of electrolysis:

1. the amount of any substance dissolved or deposited is directly proportional to the amount of electricity which has flowed.
2. the amount of different substances deposited or dissolved by the same quantity of electricity is proportional to their chemical equivalent weights. Since the electrolyte serves as the conductor of electric current, Ohm's law could be applied to this type of conductor.

The Faraday's law indicates a relation between the numbers of electrons removed from an atom and the mass of the atom that would dissolve into electrolyte. The simple expression of Faraday's law can be described as:

$$m = kIt, \text{ [1]} \tag{2.1}$$

where

k is the electrochemical equivalent of the anode metal($=A/(Z \cdot F)$ in (g/C))

m is the mass

I is the electric current (A)

T is the machining time

A is the atomic weight of dissolving ions

Z is the valence of dissolved ion immediately after dissolution

F is the Faraday's constant of 96,487 Coulombs(C)

However, instead of assumption that all current is used to ionize the workpiece atoms during the process ECM, some of the current goes into other undesirable electrochemical reactions. Therefore, an efficiency term (η), which can describe the percentage of current applied to dissolve atoms in the overall current, is necessary. By using the electrochemical equivalent equation (2.1) yields to:

$$m = \eta \cdot k \cdot I \cdot t \tag{2.2}$$

The dissolution of metal from the workpiece surface is the only useful reaction in the process of ECM and all the other reactions such as metal deposits on the tool and the production of gas contributes little to a loss of machining current. Ion dissolution valence is required in describing the dissolution electrochemical process and calculating material removal according to Faraday's law. Table 2.1 shows the dissolution valences of some

metal in different metal electrolyte. Ions valence can be varied in different solutions and process conditions.

Table 2.1 Metal dissolution valence in different metal electrolyte systems [10]

Metal	Electrolyte	Dissolution valence
Ni	NaCl	2
Ni	$NaNO_3$	2*
Fe	NaCl	2 and 3
Fe	$NaNO_3$	2*
Cr	NaCl	6
Cr	$NaNO_3$	6

*Accompanied by oxygen evolution

2.3 Valence State Estimation

Determining the accurate valence states of elements is difficult to achieve. The valence state value may not be the actual value when calculating the metal removal rate followed by Faraday's law, which reason may due to the following reasons:

1. the element may behave differently in the alloy,
2. the corrosion potential may not be an equilibrium potential and in this case the element state in the alloy may not be the equilibrium state.

Generating the potential-pH diagram and measuring the corrosion potential of the alloy are the two methods that can approximately estimate the proper valence. The estimation of corrosion current density, which is a measure of the corrosion rate, can be

obtained by applying electrochemical measurements such as polarization resistance and Tafel extrapolation appropriately [11]. The potential-pH diagram helps to estimate the most stable valence under certain conditions. The equilibrium phases of an aqueous electrochemical system are shown by using the potential-pH diagram. The X-axis refers to the pH value and the Y-axis shows the potentials. This diagram is used to predict whether or not corrosion can occur, estimate the composition of the corrosion products formed, and predict the environmental changes to prevent or reduce corrosion attack [12]. For nickel alloy, the main metal components include nickel, iron, chromium, and molybdenum and the Potential-pH diagrams for each metal are shown in figures 2.1-2.4. Potential-pH diagram for the alloy (nickel alloy ASTM B435 as workpiece) with a solid phase as a dissolution product is obtained by using THERMEXPERT - Potential-pH Diagram Generator on line [13, 14].

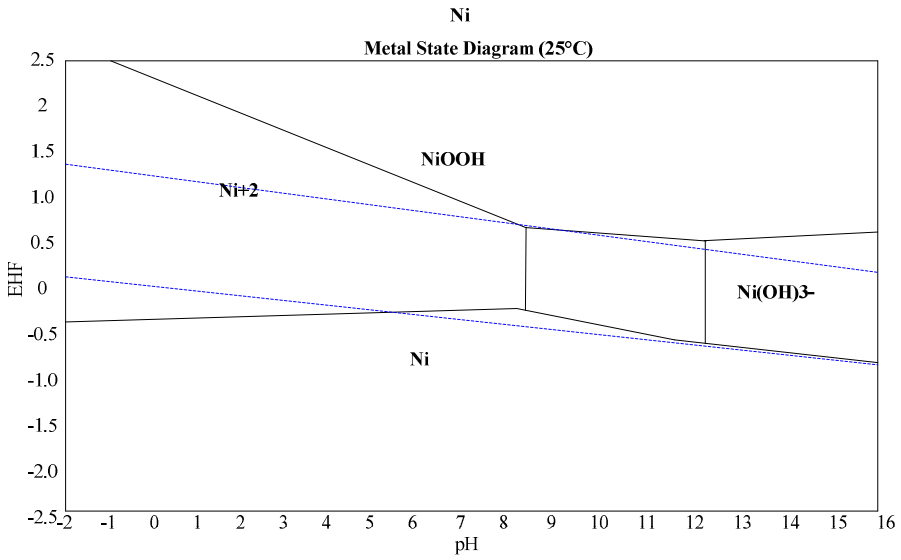

Fig. 2.1 Potential-pH diagrams for nickel in metal state [14]

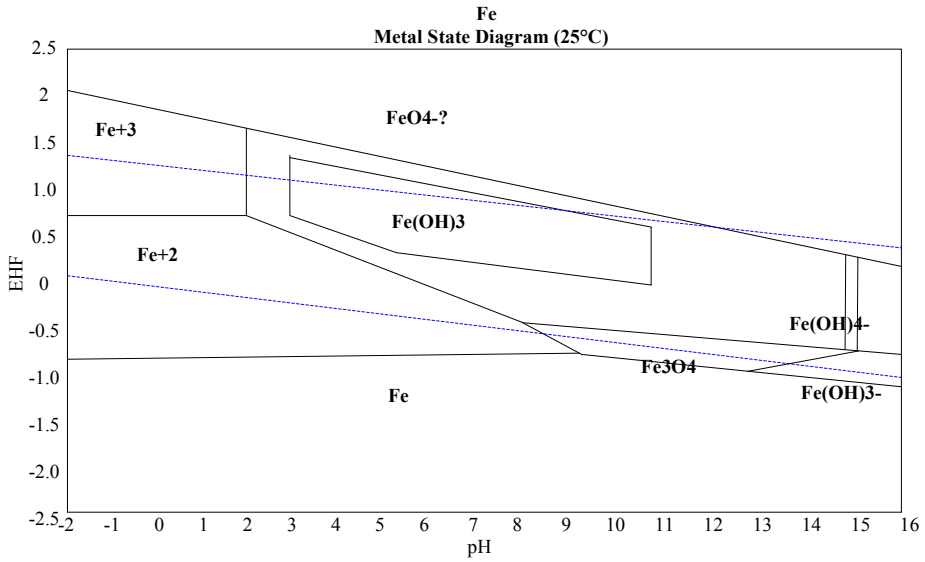

Fig. 2.2 Potential-pH diagrams for iron in metal state [14]

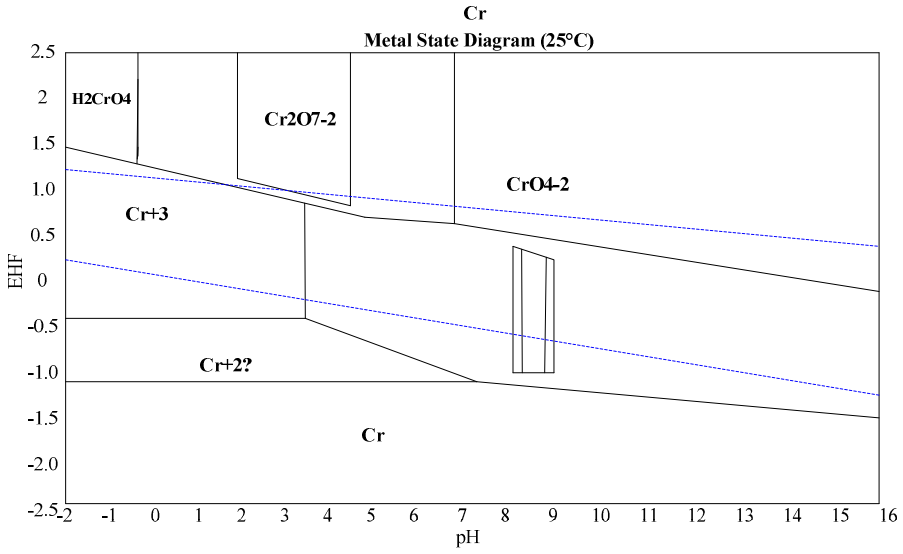

Fig. 2.3 Potential-pH diagrams for chromium in metal state [14]

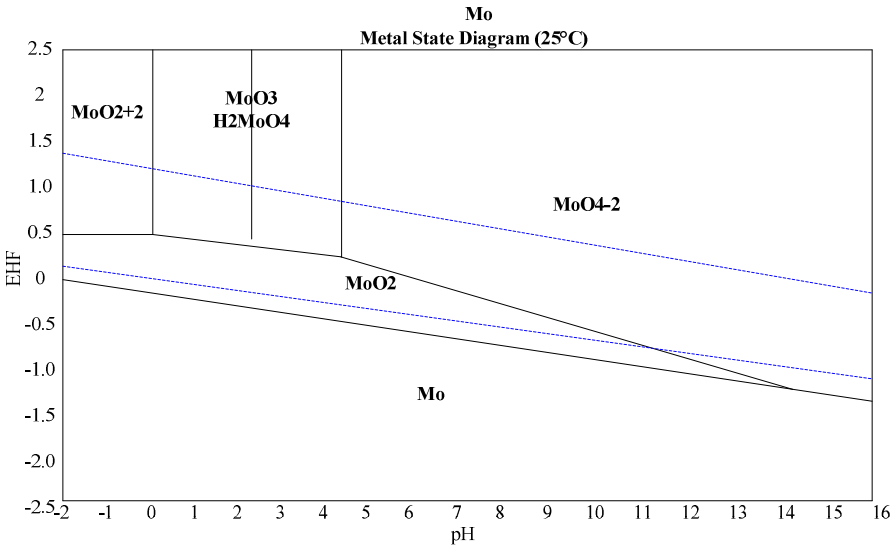

Fig. 2.4 Potential-pH diagrams for molybdenum in metal state [14]

2.4 Anode Potential

Interruption technique was used to study the anode potential of mild steel during electrochemical machining in sodium chloride solution and results show that [15]

1. the anodic current is mainly consumed in iron dissolution although there is a slight decrease in current efficiency as the current density increases.
2. the iron dissolution process is not affected by flow rate in the turbulent region, but is influenced by sodium chloride concentration.
3. in the transition region anodic film effects can be observed. The electrolyte concentration affects potential through the changes in electrolyte conductivity.

The anodic ohm potential drop and the current efficiency for electrochemical machining of mild steel in the sodium chlorate solution were studied [16]. Experiment results indicate that an oxide film appeared when current density is low and the current is consumed in oxygen generation at the anode. The oxide film would begin to disappear when increasing current density and will finally vanish in the high current density region where the metal dissolution takes place. Current efficiency measurements were carried out on mild steel in combination solution of sodium sulfate and sodium chloride. The Cl^- ions have the ability to solve the salt layer and lessen the protectiveness of the anodic film [17, 18, 19].

2.5 Types of Electrolyte

Sodium chloride is very corrosive and has a stable conductivity over a broad pH range. On the other hand, sodium nitrate is much less corrosive compared to sodium chloride. However, a passivating oxide layer creates at the workpiece surface; causing the decrease of the electrolytic process. By applying sodium chloride as an electrolyte, high machining voltage up to 5%-30% is needed to counter the electromotive force that is produced by polarization. The rest energy is used to overcome the electrolyte resistance in the machining gap. The electrolyte reactions require higher voltage when using strong passivating electrolyte like sodium nitrate.

The Cl^- ions affect the position of the active and the passive regions of the polarization curves at the low concentration range. When the Cl^- ions are added to the sodium nitrate solution, the electrolyte oxidizing power is reduced by providing the Cl^- ions competing with the NO_3^- ions for adsorption sites at the electrode surface. Therefore,

more anodic potential must be satisfied before forming the protective film. However, the alloy surface is strongly protected so the current in the passive region does not increase. Therefore, the active-passive transition is shifted to more noble potentials [1, 20].

Recently, an aqueous solution of inorganic chloride and nitrate salt has been used as electrolytes. The concentrations of these ingredients in certain electrolyte should fall within the established limits. Otherwise, intolerable defects such as unwarranted inter-granular attack and phase dissolution may appear on the electrochemically machined surface of the nickel alloy. The citric acid has been largely used to eliminate the smutting problem. This solution has a good chemical stability and can be used for a long period in the ECM with applying a proper in-process filtration. Moreover, the citric acid and the sodium citrate are completely biodegradable and do not pollute the solutions and do not cause environmental problems. Citric acid also does not emit nitrogen oxide vapors, which are harmful to the atmosphere. Nitrogen oxides aid in the production of smog, whereas citric acid does not [21, 22, 23].

2.6 Pulse Parameters

In PECM, shorter pulse on-time decreases the concentration polarization effect so that the peak current will increase, which will decrease the selective dissolution and the surface roughness. However, a certain length of pulse on-time is required for anodic surface charged or polarized to gain enough energy in order to activate the dissolution. The pulse off-time influences the resumption of the polarized anodic surface and affects anodic overpotential changes. Longer pulse off-time leads to better results of anodic surface roughness [8, 24]. The pulse parameters such as pulse on/off time affect the

current density, the anodic overpotential and the current efficiency significantly. As a result, the local anodic dissolution rate is more sensitive to the changes in the local current density, leading to higher dissolution localization and more uniform gap distribution than in the ECM with continuous current [25].

2.7 Nickel Alloy Machining Methods

Traditional machining processes such as turning, drilling, milling, and grinding have been used to machine nickel alloys [12, 26]. Since these alloys are difficult to machine using the traditional methods, the nontraditional methods have been proposed to machine these alloys. ECM is one of the nontraditional processes that has been used to machine nickel alloys. However, ECM presents a serious environmental challenge due to the production of hexavalent chromium and other heavy metal hazardous waste. The electrolyte in the electrochemical machining of nickel base super alloys was investigated to reduce the negative impact on the environment [27]. Nickel base super alloys containing additions of hafnium were used as workpiece. Very satisfactory results were obtained when chloride ions are about 0.6 to about 1.25 pounds per gallon, nitrate ions are present in the amount from 1.25 to about 2.0 pounds per gallon, and the pH of the solution being from about 8 to about 12 [28,29].

The jet and laser-jet electrochemical micromachining of nickel and steel in neutral solutions of sodium chloride and sodium nitrate were studied [30]. From the experimental results, when a laser beam is not applied, nitrate solution can obtain high machining rates and relatively low overcutting; therefore make it suitable for micromachining. If the laser beam is used in the machining process, nitrate solution is found to be inappropriate for

micromachining, since oxygen evolution process consumed most of the energy and the metal dissolution is no longer the main reaction at the anode. However, metal dissolution reaction is not affected by the absence of laser power when chloride solution is used as electrolyte. Moreover, a laser beam can increase the effective machining rate and precision by assisting the applied current focused into the machining area [29, 30]. The effect of pulsed current on anodic electrochemical behavior has been studied [31].

2.8 Current Efficiency Definition

"The current efficiency is defined as the ratio of the observed amount of metal dissolved to the theoretical amount predicted from Faraday's law, for the same specified conditions of electrochemical equivalent, current, etc. [1]" Current efficiency is commonly applied in PECM efficiency calculation. The energy efficiency considers the effect of voltage component of required power assuming current is fixed. Electrical energy efficiency is a more accurate measurement to evaluate the PECM performance than current efficiency and is based on the calculation of the energy required passing a specified current across the machining gap [1]. However, it is complicated to measure or calculate energy efficiency directly from experimental results and current efficiency is easier and more convenient to illustrate than energy efficiency, thus current efficiency is applied in this investigation.

2.9 Factors Influencing Current Efficiency

In practice other side reactions may exist, like oxygen and chlorine precipitation from anode; some metal dissolved as high valence ion thus extra quantity of electric

charge will be consumed. The amount of electrolyzed metal will be smaller than the theoretical value sometimes. Figure 2.5 indicates the factors influencing current efficiency. Electrical conductivity played a crucial role in current efficiency. Heat transfer, electrolyte flow, electrode structural geometry, and mass balance may affect electrical conductivity by heat generation, products flush, electrode position, and gas generation respectively.

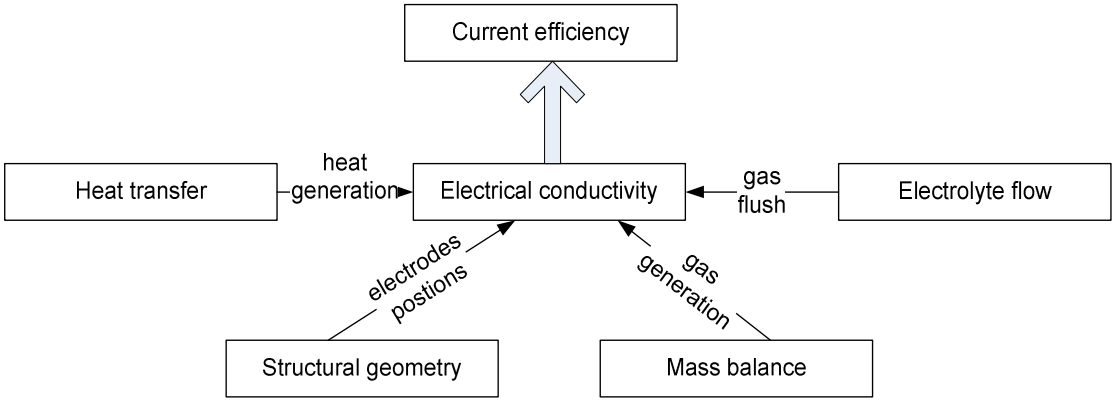

Fig. 2.5 Factors influencing current efficiency

CHAPTER3

EXPETIMETS AND RESULTS

3.1 Experimental Objectives

To study the current efficiency of PECM, it is necessary to identify and understand the factors affecting the current efficiency. The factors affecting the current efficiency have been studied by conducting series of machining experiments using nickel alloy as workpiece. Nickel alloys have several applications including high temperature resistant applications, shape memory applications, and wet corrosion applications, such as exhaust nozzles, nickel foams, solid-oxide fuel cells. The experimental setup of the PECM has been shown in the Section 3.2. The effect of the different process parameters such as the electrolyte and its flow rate, current density, duty cycle and pulse on-time has been studied and has been reported in the following chapters. The results have been analyzed and presented in the Section 3.4. The statistical analysis conducted by SPSS has been shown in the Section 3.5.

3.2 Experimental Setup

The experimental setup consists of a pulse/DC power supply, a relay with digital timer, a personal computer with USB data acquisition device, an electrolyte holding tank (~1L), the electrolyte, a workpiece fixture, a vertical slide with stepper motor, and a pump drive with pressure gauge. Figure 3.1 shows the PECM setup used for the experiments.

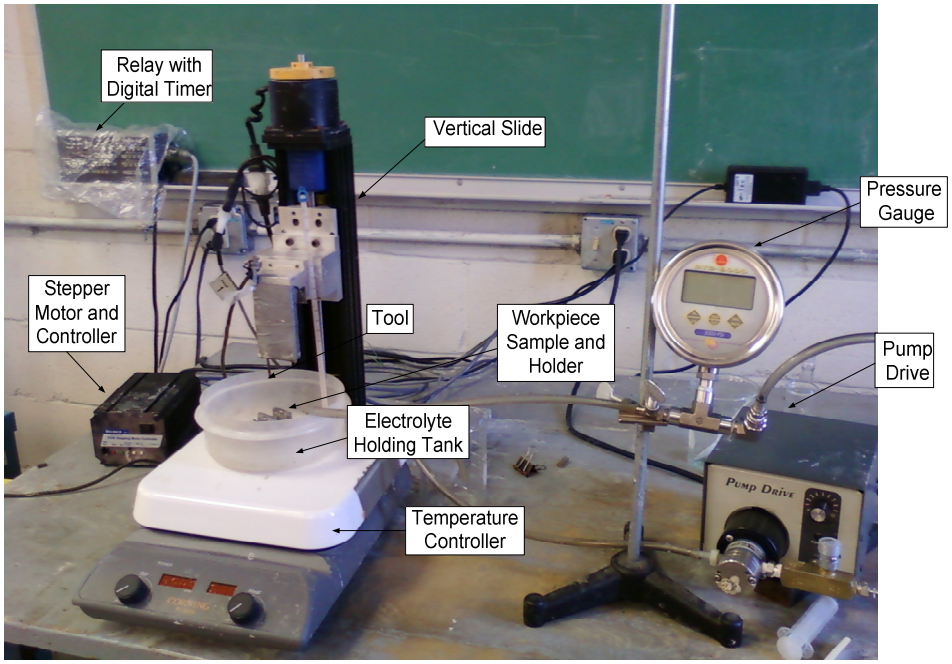

Fig. 3.1 The electrochemical machining system

The power supply manufactured by Rapid Power Technologies Inc. is capable of generating both constant current and constant voltage. The average current produced in DC mode is 100 amps. The power supply is rated at a peak current of 200 amps in pulse mode. It provides up to 30 volts in pulse mode. Moreover, the pulse on/off-time can be set to desired amount ranging from 0.1 to 100 milliseconds. The voltage can be set directly through the control knobs.

The Gralab 645 Digital timer that connected to a relay is capable to provide the accurate machine time. The digital timer can be programmed to correct length of machining time from 0.1 second to 99 hours 99 minutes and 9 seconds.

The vertical slide and the stepper motor controller are manufactured by Velmex Inc. and are capable to place accurate tool electrode placement and movement. They are

used to set the initial interelectrode gap and keep electrode stationary during every experiment. One rotation of the shaft movement (cause the tool electrode move up or down 2mm) requires 400 pulses from the controller, which means each pulse contributes to tool electrode movement of 5μm.

There is a need for temperature control of experiments. This is accomplished by a Corning PC-620D stirring hot plate with a 10" x 10" (25.4 x 25.4cm) Pyroceram top and a digital temperature display. The digital hot plate offers consistent and repeatable temperature settings from 5°C (if ambient temperature is 0°C or lower) up to 550°C. The digital LED temperature display is adjustable in 5°C increments and blinks until set temperature is reached. Meanwhile, a thermometer (range from 0 to 200 °F) is used to measure the electrolyte temperature.

The workpiece sample material: nickel alloy, which is ASTM B435 (UNS N06002), has the composition by % weight: Cr - 20.5%-23.0%, Fe - 17.0%-20.0%, Mo - 8.0%-10.0%, and Ni – Remainder. The nickel alloy was cut into small pieces of 1.25cm by 1.25cm under the help from engineering and science research support facility in University of Nebraska.

The interelectrode gap was usually set from 0.025 to 0.76mm according to literature. The gap could only be set in 0.005mm increments and the value of 0.05mm was chosen in this experiments.

Figure 3.2 is a simplified schematic of the ECM cell apparatus. The electrolyte flow direction, which is from the right of the workpiece to the left with a certain rate flushing away products of the electrochemical reaction with the heat generated in the process. Possible electrochemical reactions of nickel alloy as workpiece and sodium

chloride and/or sodium nitrate as electrolyte are shown in figure 3.3. The current efficiency is calculated as [1]:

$$\eta_{current\ efficiency} = \frac{mass\ before\ maching - experimental\ mass\ after\ machining}{theoretical\ amount\ predicted\ from\ Faraday's\ law\ (kIt)} \times 100\% \quad (3.1)$$

where k is the average electrochemical equivalent of the workpiece and can be calculated as equation 3.2[1]. Energy consumption per unit material removal is studied under different experimental conditions and each condition has one replicate to determine the optimum combination of process parameters to achieve energy efficiency.

$$k = \frac{1}{F\left(\frac{n_1 a_1}{A_1} + \frac{n_2 a_2}{A_2} + \frac{n_3 a_3}{A_3} + \cdots\right)} \quad (3.2)$$

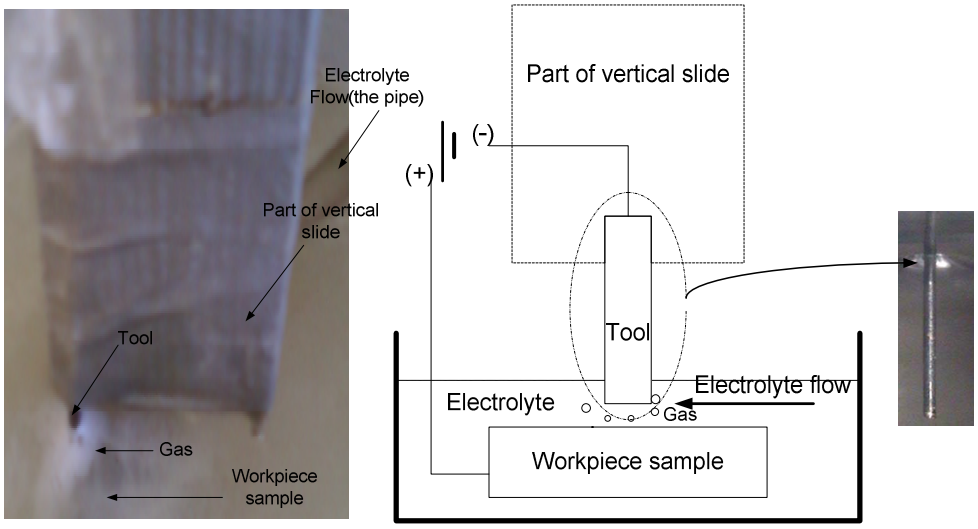

Fig. 3.2 Principle scheme of electrochemical machining

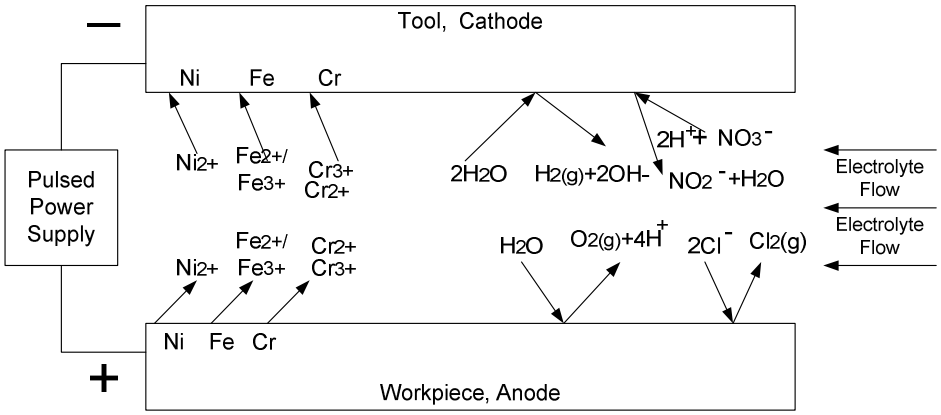

Fig. 3.3 Possible electrochemical reactions

3.3 Experimental Design

A continuous D.C. voltage (7-25 volts) is usually applied with the current density ranging from an order of 10 A/cm2 to 103 A/cm2. Electrolyte (typically NaCl or $NaN0_3$ aqueous solutions) is supplied to flow through the gap with a high velocity of 10-60 m/s to maintain the electrochemical dissolutions on the workpiece surface and to flush away the waste products and heat generated during the electrochemical reactions. The anodic electrochemical dissolution occurs during the short pulse on-times, each ranging from 0.1 ms to 5 ms [25, 32].

3.3.1 Screening Design Experiment

The preliminary design of experiments is the feasibility study and conducted to reduce the number of parameters for next randomized experiment by analyzing their statistical significance on current efficiency. Eight variables are chosen in the screening design experiment including duty cycle, pulse on-time, machining time, temperature, type

of electrolyte, electrolyte concentration, electrolyte flow rate, and current density. There are two levels for each parameter making up a 16 run geometric design experiment. Table 3.1 indicates the parameters with low and high levels. The 16 run geometric design with experimental results is shown in table 3.2. Parameters and their ranges were chosen based on literature and machine limitation.

Table 3.1 List of factors and their levels for the screening design experiment

Factors	Labels	Low level setting (-1)	High level setting (+1)
Duty cycle($\frac{\text{On time}}{\text{On+off time}}$)	A	40%	80%
Pulse on- time	B	5ms	30ms
Machining time	C	4min	8min
Temperature	D	25℃	35℃
Type of electrolyte	E	$NaNO_3$	$NaNO_3$ +citric acid
Electrolyte concentration (weight %, water as solvent)	F	$NaNO_3$10%	$NaNO_3$ 20%
Electrolyte flow rate	G	0ml/min	2500ml/min
Current density	H	3.2 A/cm^2	51.2A/cm^2

Table 3.2 Design matrix of a 16 run geometric design and experimental results

Run	A	B	C	D	E	F	G	H	η (current efficiency %)
1	1	1	1	1	1	1	1	1	12.21
2	1	1	-1	1	-1	-1	-1	1	9.08
3	1	-1	1	-1	1	-1	-1	1	11.63
4	1	-1	-1	-1	-1	1	1	1	14.92
5	-1	1	1	-1	-1	1	-1	1	15.95
6	-1	1	-1	-1	1	-1	1	1	16.2
7	-1	-1	1	1	-1	-1	1	1	9.35
8	-1	-1	-1	1	1	1	-1	1	9.77
9	-1	-1	-1	-1	-1	-1	-1	-1	13.81
10	-1	-1	1	-1	1	1	1	-1	16.2
11	-1	1	-1	1	-1	1	1	-1	10.36
12	-1	1	1	1	1	-1	-1	-1	15.95
13	1	-1	-1	1	1	-1	1	-1	14.92
14	1	-1	1	1	-1	1	-1	-1	11.28
15	1	1	-1	-1	1	1	-1	-1	9.15
16	1	1	1	-1	-1	-1	1	-1	9.06

3.3.2 Randomized Experiment

Based on the results from the preliminary experiments, factors having significant effects on current efficiency need further examined with the purpose of improving current efficiency. This randomized experiment aims to supplement the first set of experiment and expects more information about the interrelationships between different factors. The four kinds of electrolyte from the last experiment were continuing used and the other parameters in this experiment cover electrolyte flow rate, and current density. Table 3.3 indicates different levels for each factor and experimental results.

Table 3.3 List of factors and experimental results

Flow rate	Current density	E1 ($NaNO_3$ 10%)	E2 ($NaNO_3$10% +citric acid 10%)	E3 ($NaNO_3$ 20%)	E4 ($NaNO_3$20% +citric acid 10%)
		Current efficiency (%)			
500ml/min	3.2A/cm^2	12.54	12.32	15.92	14.33
	6.4A/cm^2	8.87	8.79	12.33	12.56
	12.8A/cm^2	19.03	18.56	22.81	23.46
	25.6A/cm^2	36.78	37.95	48.95	49.06
	51.2A/cm^2	23.56	31.5	31.25	44.72
1000ml/min	3.2A/cm^2	11.86	10.8	15.25	14.67
	6.4A/cm^2	10.55	9.86	13.38	12.56
	12.8A/cm^2	20.33	18.96	25.25	26.75
	25.6A/cm^2	38.25	37.96	50.68	44.23
	51.2A/cm^2	37.85	38.25	28.86	36.78
1600ml/min	3.2A/cm^2	14.92	11.96	18.7	14.92
	6.4A/cm^2	9.35	10.55	11.96	10.36
	12.8A/cm^2	18.32	20.46	23.45	25.64
	25.6A/cm^2	40.13	41.25	54.68	56.87
	51.2A/cm^2	60.16	61.86	74.75	77.83
2500ml/min	3.2A/cm^2	14.92	12.31	18.2	16.43
	6.4A/cm^2	10.36	10.67	9.77	9.31
	12.8A/cm^2	20.64	16.74	30.1	20.56
	25.6A/cm^2	46.87	39.5	45.13	44.78
	51.2A/cm^2	64.83	56.63	70.1	60.34

3.4 Results

In the screening design experiment, parameters having significant influence on current efficiency were chosen after running variable analysis through Statistical Package for the Social Sciences (SPSS) and the results are shown in figure 3.4:

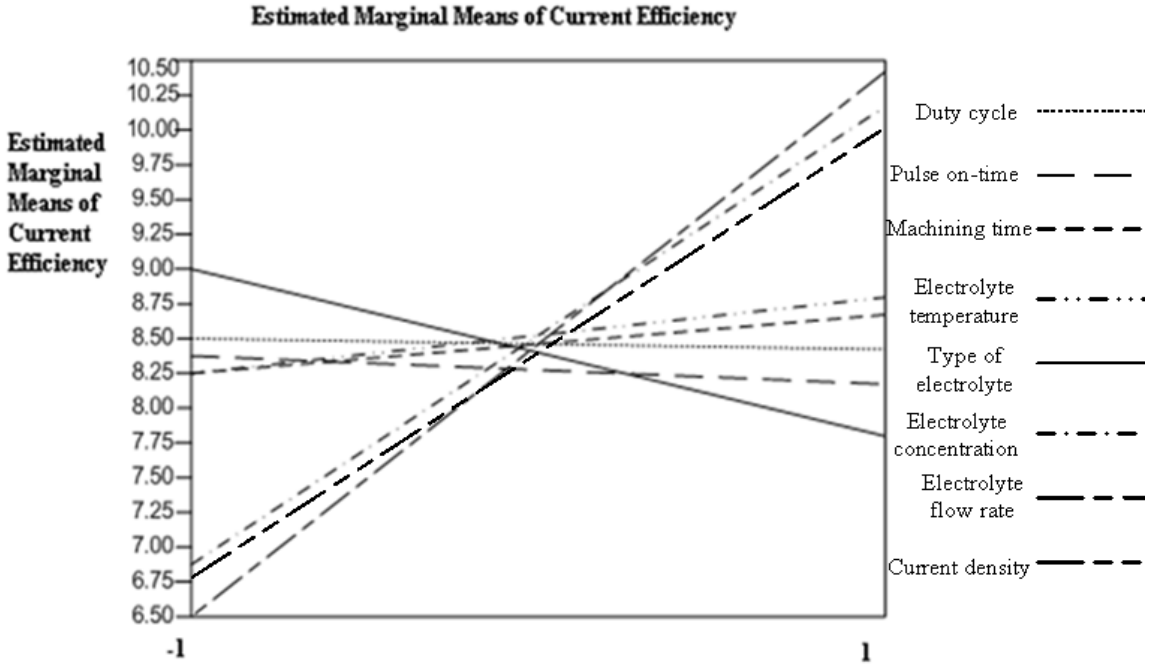

Fig. 3.4 Relations between estimated marginal means of current efficiency and variable parameters

It can be seen from the result that type of electrolyte, electrolyte concentration, electrolyte flow rate, and current density affect the current efficiency significantly. Increased machining time, temperature, and electrolyte flow rate lead to higher current efficiency. The small duty cycle, short pulse on-time, long machining time and high electrolyte temperature make higher current efficiency possible, meanwhile, sodium nitride with higher concentration guides to higher current efficiency compared with sodium chloride.

3.4.1 Effect of Current Density

The overall effects of current density on current efficiency are shown in figures 3.5-3.8 separately. The current efficiency achieved with increasing current density was

almost increased. However, there was an exception when current density increased from 3.2A/cm^2 to 6.4A/cm^2. In this case, current efficiency decreased but not significantly.

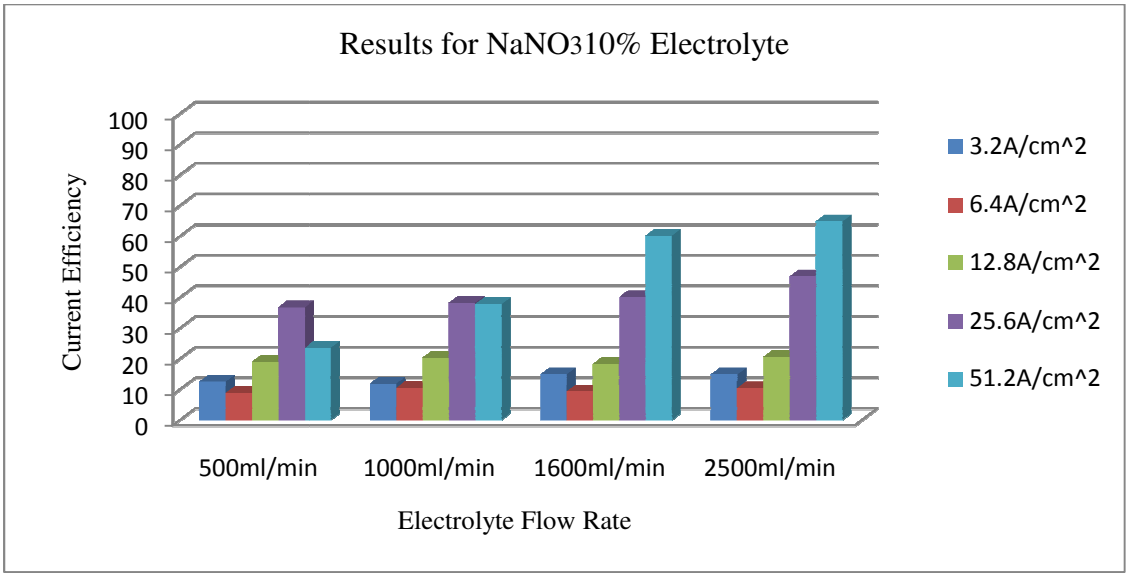

Fig. 3.5 Results for $NaNO_3$10% Electrolyte: Effect of Flow Rate and Current Density

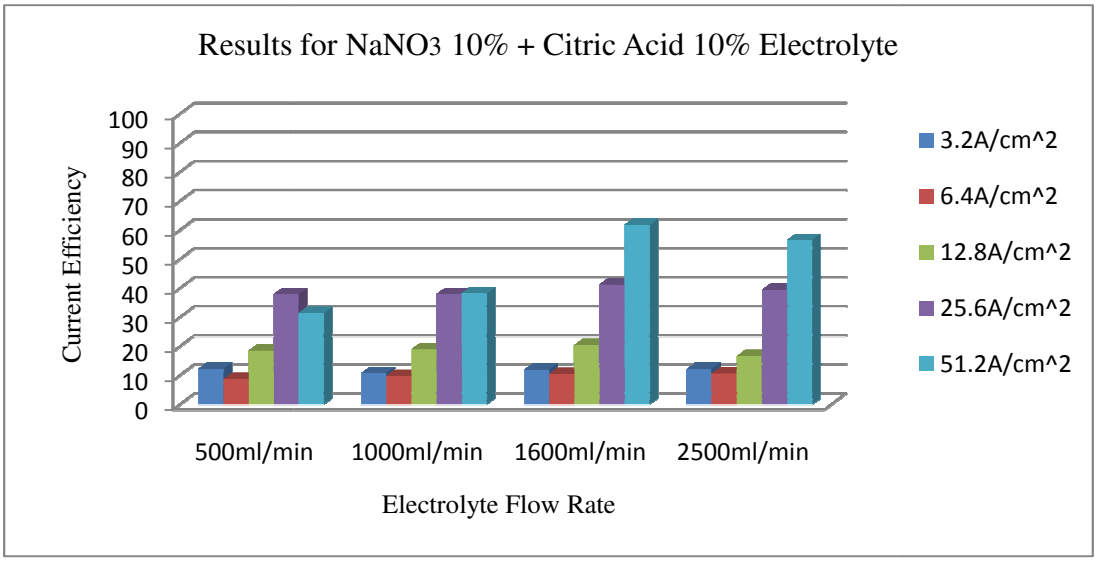

Fig. 3.6 Results for $NaNO_3$10% + Citric Acid 10% Electrolyte: Effect of Flow Rate and Current Density

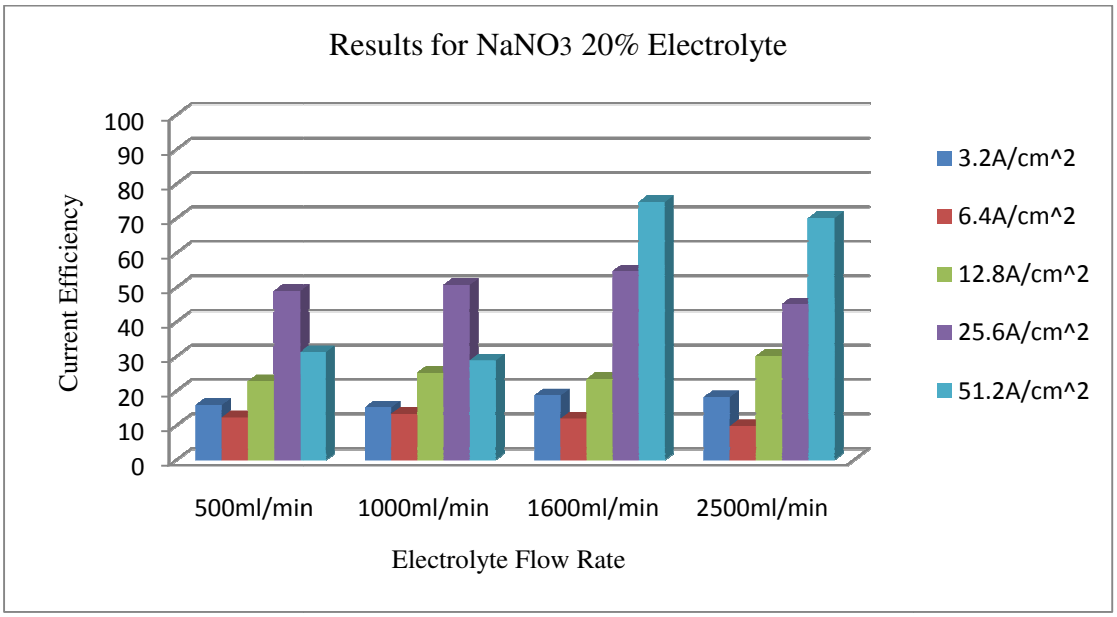

Fig. 3.7 Results for $NaNO_3$20% Electrolyte: Effect of Flow Rate and Current Density

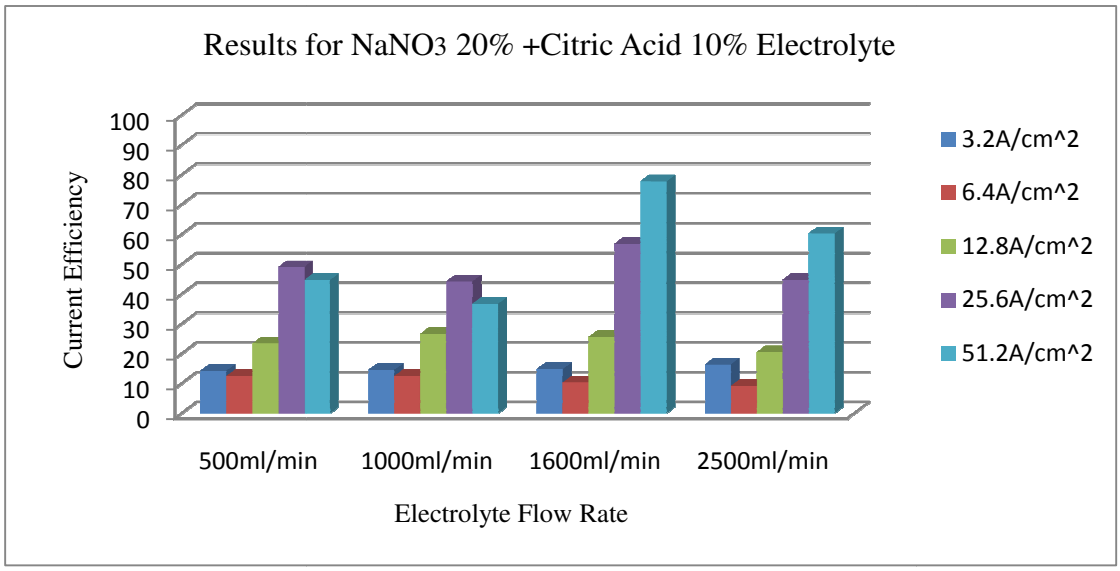

Fig. 3.8 Results for $NaNO_3$20% + Citric Acid 10% Electrolyte: Effect of Flow Rate and Current Density

3.4.2 Effect of Electrolyte Flow Rate

The current efficiency was reduced when the rates of the flow were kept low. Insufficient flow does not allow the products of machining to be so readily flushed from the machining gap.

3.4.3 Effect of Electrolyte

By comparing E_1 ($NaNO_3$10%) and E_2 ($NaNO_3$10%+ citric acid 10%) as well as E_3 ($NaNO_3$20%) andE_4($NaNO_3$20% + citric acid 10%) from figure 3.9 and 3.10, the current efficiency decreased when citric acid was added to sodium nitride. Citric acid is a weak acid and not easy to form anions and cations, so the anodic dissolution is slowed down. The current efficiency increased when sodium nitride concentration increased by comparing E_1 ($NaNO_3$10%) and E_3($NaNO_3$20%). Increased electrolyte concentration can cause electrolyte conductivity increase for some electrolytes, and the electrolyte conductivity is inversely proportional to the resistance drop (IR), which is a component of voltage drop across a PECM cell. Therefore, the required voltage, hence the power (as the current is fixed) can be decreased. In this case, the required power will be decreased and higher energy efficiency achieved.

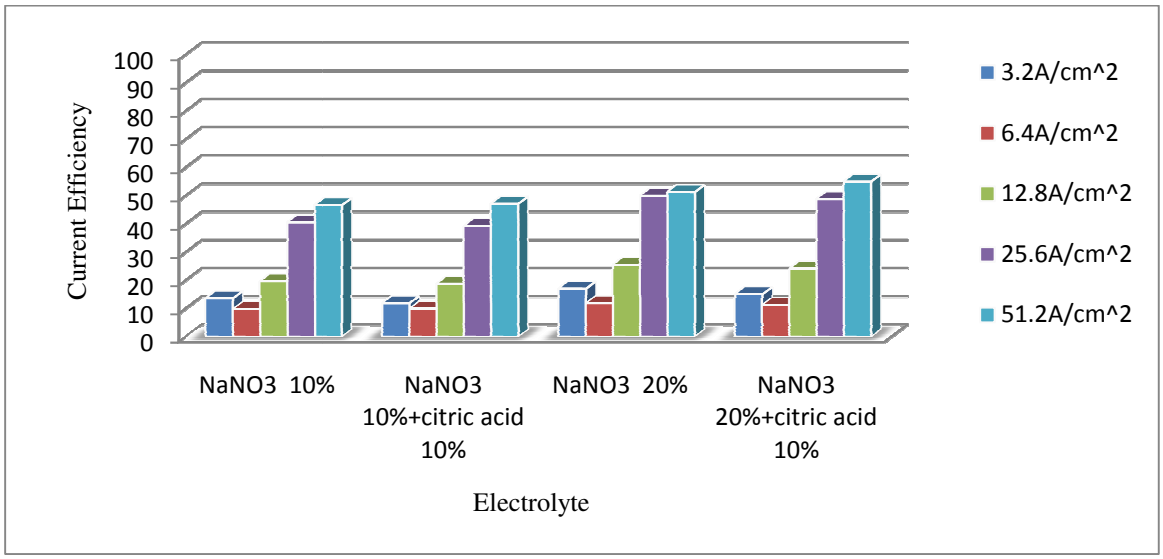

Fig. 3.9 Current Efficiency Results: Effect of Electrolyte and Current Density

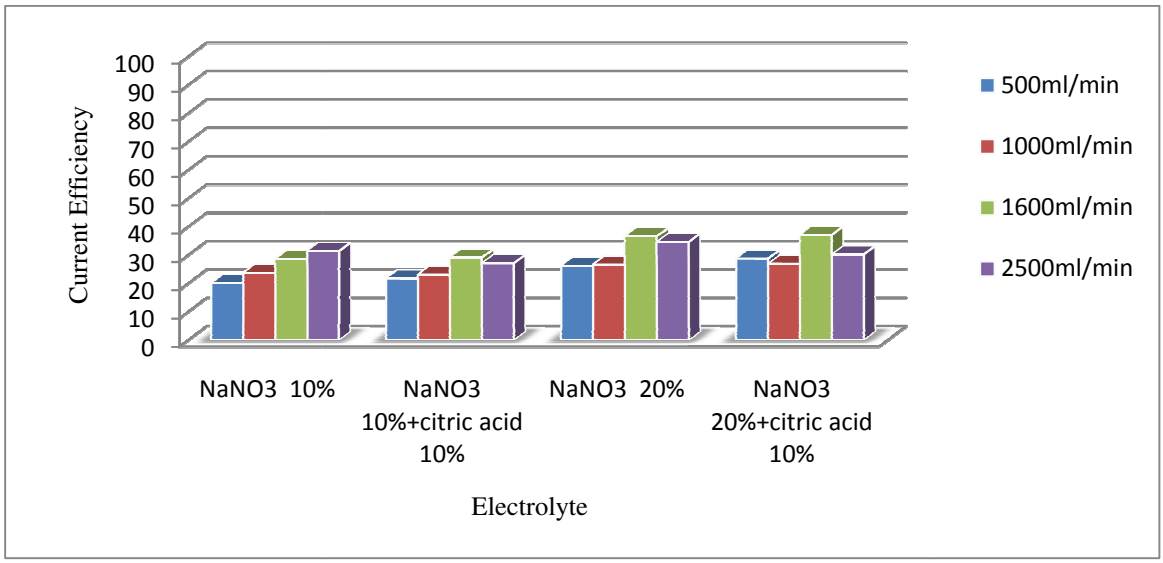

Fig. 3.10 Current Efficiency Results: Effect of Electrolyte and Flow Rate

In conclusion, current efficiency was higher when applying a faster electrolyte flow rate for all of the four kinds of electrolyte. However, the current efficiency decreased indistinctly when a flow rate increased from 1600ml/min to 2500ml/min. The

electrolyte flow flushes away the increasing contamination of reaction products, which cut off workpiece material dissolution. A higher current density almost led to higher current efficiency for all the electrolyte cases, whereas, the current efficiency was always decreased when a current density increased from 3.2A/cm^{2}to 6.4A/cm^2. Choice of electrolyte did not significantly affect the current efficiency, as seen from figure 3.9 and 3.10. A higher electrolyte concentration led to a higher current efficiency.

3.5 Statistical Analysis

A model for predicting and simplifying the relations between current efficiency and the variables electrolyte, electrolyte flow rates, and current density after analyzing their complex relations and interactions is developed here. All statistical analyses were carried out on the Statistical Package for the Social Sciences (SPSS). The regression analyses were performed using the stepwise regression procedure with alpha equal to 0.05. Three ANOVAs were used – one with all variables included and one each for each of the two kinds of electrolyte. Additionally, three regression analyses were conducted – one with all variables and one each for each of the two kinds of electrolyte.

The results from ANOVA indicate whether the classes of variables have different effects on current efficiency. However, ANOVA cannot give quantitative relationships between the parameters. Therefore, regression analysis was applied to the data to quantitatively determine the specific relationships between the variables and their interactions. The regression procedure was applied to determine the experimental behavior of the current efficiency after PECM by varying the parameters electrolyte

concentration(*C*), electrolyte flow rate (*V*), current density (*J*) and interactions among the various parameters.

3.5.1 Statistical Analysis of Current Efficiency with Two Kinds of Electrolyte

This analysis was done on two kinds of electrolyte, two levels of concentration (*C*), four levels of electrolyte flow rate (*V*), and five levels of current density (*J*). The categories of electrolyte (*E*) were $NaNO_3$ electrolyte (represented by "0") and $NaNO_3$ & citric acid (represented by "1"). Electrolyte concentration (*C*) levels were 10% and 20%. The electrolyte flow rate (*V*) levels were 500ml/min, 1000ml/min, 1600ml/min, and 2500ml/min. The five levels of current density (*J*) were 3.2A/cm^2, 6.4/cm^2, 12.8A/cm^2, 25.6A/cm^2, and 51.2A/cm^2.

ANOVA

The initial model that was investigated in the general form of the four factor analysis of variance (ANOVA) model for this study was:

$$\eta=\mu+E+C+V+J+E*C+E*V+E*J+C*V+C*J+V*J+\varepsilon \quad (3.3)$$

where,

η is the current efficiency

E is the electrolytes

C is the electrolyte concentration (weight %)

V is the electrolyte flow rate (ml/min)

J is the current density (A/cm^2)

*E*C* is the interaction term between electrolyte and its concentration

*E*V* is the interaction term between electrolyte and its flow rate

*E*J* is the interaction term between electrolyte and current density

C∗V is the interaction term between concentration and flow rate

*C*J* is the interaction term between concentration and current density

*V*J* is the interaction term between flow rate and current density

The ANOVA results are shown in table 3.4 along with the results of the Duncan Multiple Range tests for *V* and *J*. The results show that electrolyte was not significant and that *C, V, J, E*V, C*J*, and *V*J* were significant. The Duncan tests showed two groupings for the *V* levels and that all levels of *J* differed significantly. The three interaction graph pairs indicate that the interactions are not just significant but important.

Table 3.4 ANOVA results for two kinds of electrolytes

Tests of Between-Subjects Effects

Dependent Variable: Y

Source	Type II Sum of Squares	df	Mean Square	F	Sig.
Corrected Model	25584.281[a]	36	710.674	64.194	.000
Intercept	64109.694	1	64109.694	5790.909	.000
E	4.325	1	4.325	.391	.535
C	554.826	1	554.826	50.116	.000
V	1084.140	3	361.380	32.643	.000
J	20439.506	4	5109.877	461.566	.000
E * C	.776	1	.776	.070	.792
E * V	114.932	3	38.311	3.461	.024
E * J	37.219	4	9.305	.840	.507
C * V	86.971	3	28.990	2.619	.063
C * J	141.669	4	35.417	3.199	.022
V * J	3119.917	12	259.993	23.485	.000
Error	476.042	43	11.071		
Total	90170.017	80			
Corrected Total	26060.323	79			

a. R Squared = .982 (Adjusted R Squared = .966)

Table 3.5 Duncan test result of electrolyte flow rate (*V*) for two kinds of electrolytes

Duncan[a,b]

V	N	Subset 1	Subset 2
500	20	24.2645	
1000	20	25.1540	
2500	20		30.9095
1600	20		32.9060
Sig.		.403	.064

Means for groups in homogeneous subsets are displayed.
Based on Type II Sum of Squares
The error term is Mean Square(Error) = 11.071.
a. Uses Harmonic Mean Sample Size = 20.000.
b. Alpha = .05.

Table 3.6 Duncan test result of current density (*J*) for two kinds of electrolytes

Duncan[a,b]

J	N	Subset 1	Subset 2	Subset 3	Subset 4	Subset 5
6.4	16	10.7019				
3.2	16		14.3781			
12.8	16			21.9413		
25.6	16				44.5669	
51.2	16					49.9544
Sig.		1.000	1.000	1.000	1.000	1.000

Means for groups in homogeneous subsets are displayed.
Based on Type II Sum of Squares
The error term is Mean Square(Error) = 11.071.
a. Uses Harmonic Mean Sample Size = 16.000.
b. Alpha = .05.

Fig. 3.11 Plots of current efficiency (*Y*) and variables of electrolyte (*E*), concentration (*C*), electrolyte flow rate (*V*), and current density (*J*) for two kinds of electrolytes

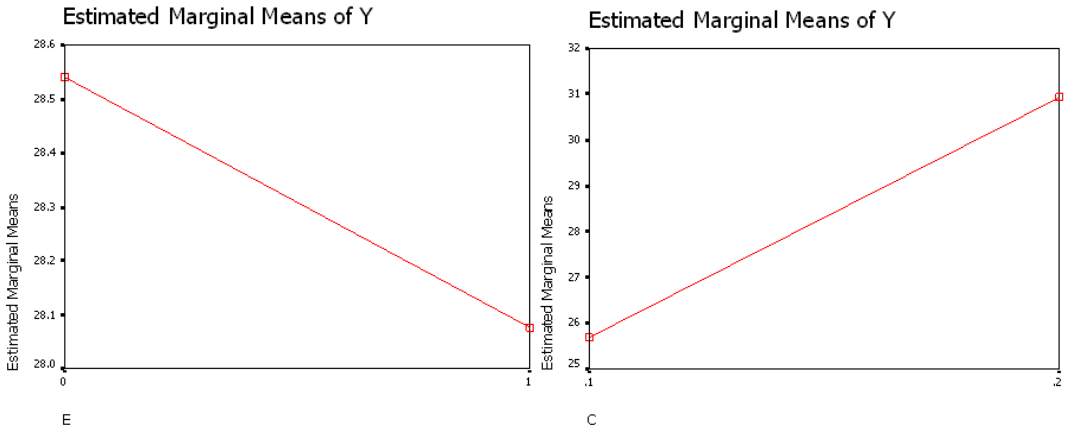

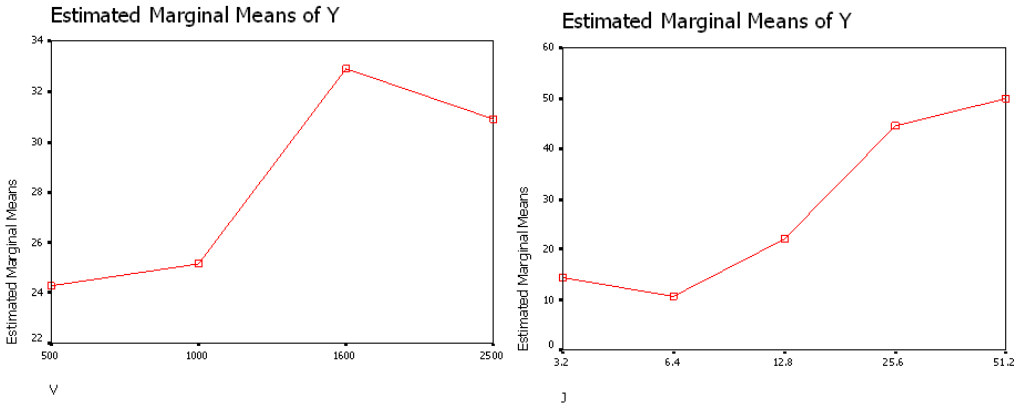

Fig. 3.12 Plots of current efficiency (*Y*) and two-way terms (*E*V, C*J,* and *V*J*) for two kinds of electrolytes

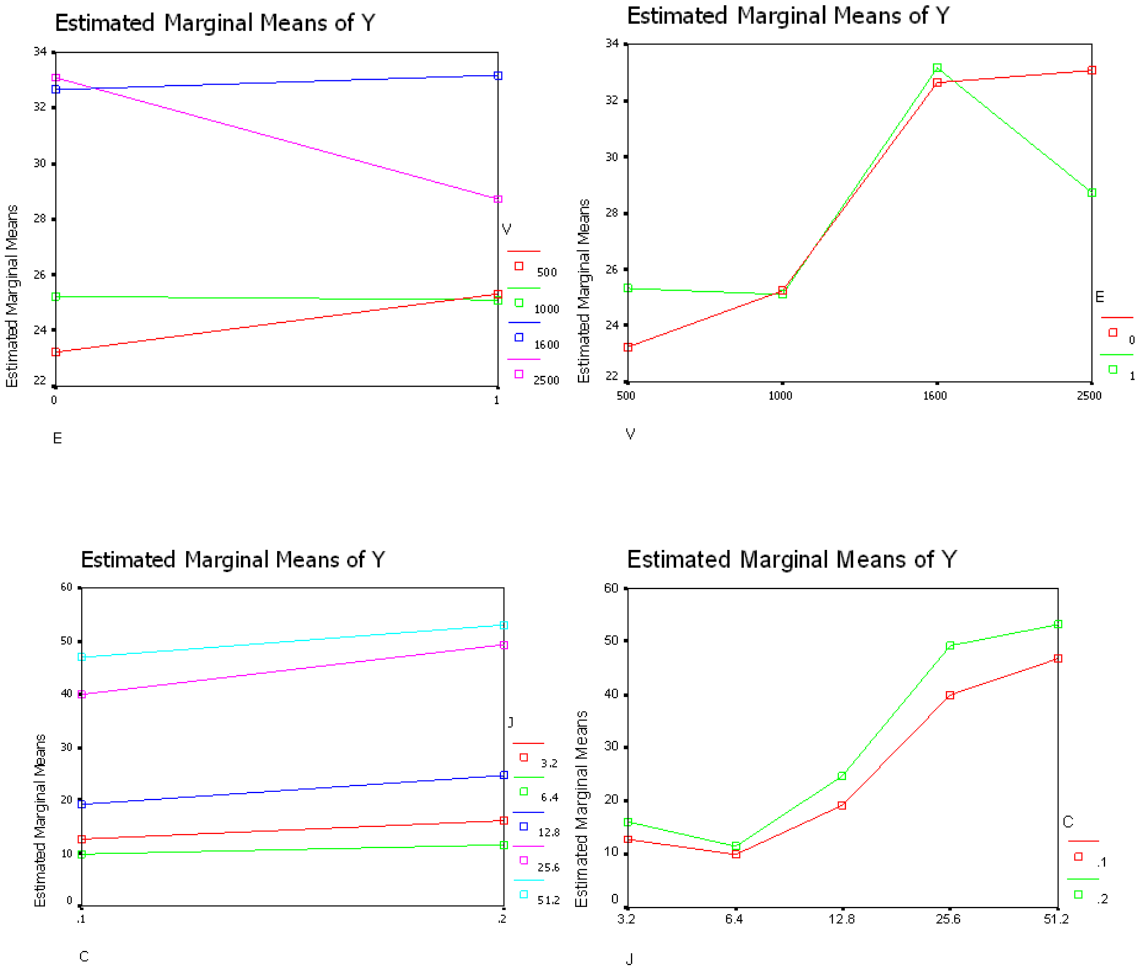

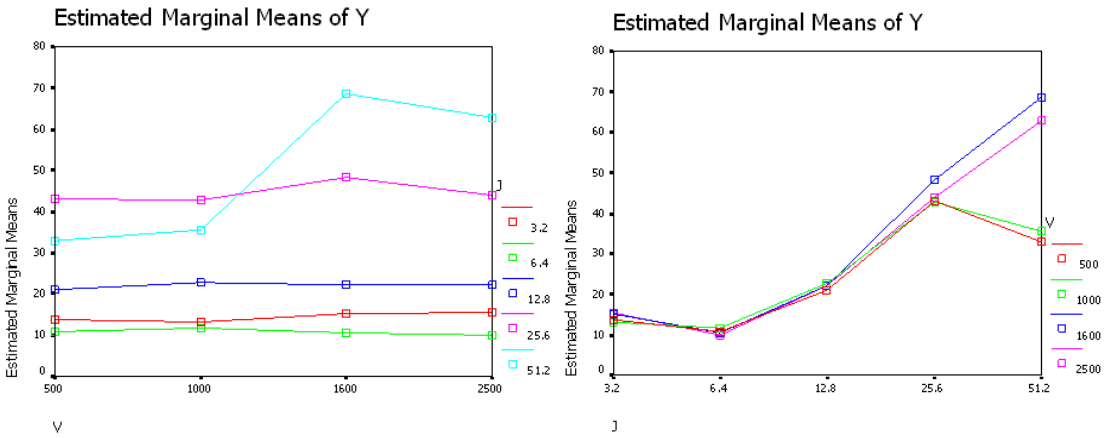

The graphs of the means for the four levels of flow rate are not parallel, and the graphs of the means for the two levels of electrolytes are also not parallel in the first two plots in figure 3.12, implying that the interactions would be considered important interactions. The graphs of the means for the five levels of current density are not parallel, and graphs of the means for the two levels of electrolyte concentration are also not parallel in the third and forth plots in figure 3.12, implying that the interactions would be considered important interactions. The means curves for the five levels of current density are not parallel, and the means curves for the four levels of flow rate are also not parallel in the last two plots in figure 3.12 , implying that the interactions would therefore be considered important interactions.

Linear Regression Analysis

For the stepwise linear regression for this study all of the variables included in the ANOVA model and the squared values of *C, V*, and *J* were included as potential variables.

The results of the stepwise regression analysis are shown in table 3.7 with the final model having five significant parameters including current density (J) and four two-way interaction terms (J^2, $V*J$, V^2, *and* $C*J$). This model is given by:

$$\eta = 5.938 + 1.253J + 3.753\times 10^{-4} V*J + 1.877 C*J - 1.239\times 10^{-6} V^2 - 2.204\times 10^{-2} J^2 \quad (3.4)$$

Table 3.7 Regression results from SPSS for two kinds of electrolyte

Model Summary[f]

Model	R	R Square	Adjusted R Square	Std. Error of the Estimate
1	.819[a]	.671	.667	10.48790
2	.875[b]	.765	.759	8.91033
3	.884[c]	.782	.773	8.64937
4	.895[d]	.802	.791	8.30206
5	.925[e]	.856	.846	7.11786

a. Predictors: (Constant), VJ
b. Predictors: (Constant), VJ, CJ
c. Predictors: (Constant), VJ, CJ, VV
d. Predictors: (Constant), VJ, CJ, VV, JJ
e. Predictors: (Constant), VJ, CJ, VV, JJ, J
f. Dependent Variable: Y

ANOVA[f]

Model		Sum of Squares	df	Mean Square	F	Sig.
1	Regression	17480.634	1	17480.634	158.921	.000[a]
	Residual	8579.689	78	109.996		
	Total	26060.323	79			
2	Regression	19946.983	2	9973.492	125.620	.000[b]
	Residual	6113.340	77	79.394		
	Total	26060.323	79			
3	Regression	20374.642	3	6791.547	90.782	.000[c]
	Residual	5685.681	76	74.812		
	Total	26060.323	79			
4	Regression	20891.014	4	5222.754	75.775	.000[d]
	Residual	5169.309	75	68.924		
	Total	26060.323	79			
5	Regression	22311.196	5	4462.239	88.075	.000[e]
	Residual	3749.127	74	50.664		
	Total	26060.323	79			

a. Predictors: (Constant), VJ
b. Predictors: (Constant), VJ, CJ
c. Predictors: (Constant), VJ, CJ, VV
d. Predictors: (Constant), VJ, CJ, VV, JJ
e. Predictors: (Constant), VJ, CJ, VV, JJ, J
f. Dependent Variable: Y

Table 3.8 Linear regression models and exclude variables result for two kinds of electrolyte

Coefficients[a]

Model		Unstandardized Coefficients		Standardized Coefficients		
		B	Std. Error	Beta	t	Sig.
1	(Constant)	15.225	1.566		9.723	.000
	VJ	4.710E-04	.000	.819	12.606	.000
2	(Constant)	12.141	1.441		8.426	.000
	VJ	2.999E-04	.000	.521	6.790	.000
	CJ	2.634	.473	.428	5.574	.000
3	(Constant)	14.940	1.824		8.191	.000
	VJ	3.860E-04	.000	.671	6.894	.000
	CJ	1.993	.531	.324	3.752	.000
	VV	-1.306E-06	.000	-.167	-2.391	.019
4	(Constant)	14.865	1.751		8.489	.000
	VJ	4.872E-04	.000	.847	7.468	.000
	CJ	3.094	.649	.503	4.765	.000
	VV	-1.942E-06	.000	-.249	-3.386	.001
	JJ	-6.320E-03	.002	-.346	-2.737	.008
5	(Constant)	5.938	2.258		2.630	.010
	VJ	3.753E-04	.000	.653	6.276	.000
	CJ	1.877	.602	.305	3.117	.003
	VV	-1.239E-06	.000	-.159	-2.433	.017
	JJ	-2.204E-02	.004	-1.208	-6.176	.000
	J	1.253	.237	1.212	5.294	.000

3.5.2 Statistical Analysis of Current Efficiency with Electrolyte of $NaNO_3$

This analysis was done on two levels of concentration (*C*), four levels of electrolyte flow rate (*V*), and five levels of current density (*J*). Electrolyte concentration (*C*) levels were 10% and 20%. The electrolyte flow rate (*V*) levels were 500ml/min, 1000ml/min, 1600ml/min, and 2500ml/min. The five levels of current density (*J*) were 3.2A/cm^2, 6.4/cm^2, 12.8A/cm^2, 25.6A/cm^2, and 51.2A/cm^2.

ANOVA

The initial model that was investigated in the general form of the three factor analysis of variance (ANOVA) model for this study was:

$$\eta=\mu+C+V+J+C*V+C*J+V*J+\varepsilon \qquad (3.5)$$

The ANOVA results are shown in table 3.9 along with the results of the Duncan Multiple Range tests for *V* and *J*. The results show that *V, J,* and *V*J* were significant. The Duncan tests showed two groupings for the *V* levels and that all levels of *J* differed significantly. The interaction graph pair indicate that the interactions are not just significant but important.

Table 3.9 ANOVA results for electrolyte of $NaNO_3$

Tests of Between-Subjects Effects

Dependent Variable: Y

Source	Type II Sum of Squares	df	Mean Square	F	Sig.
Corrected Model	12968.451[a]	27	480.313	29.064	.000
Intercept	32583.547	1	32583.547	1971.660	.000
C	257.049	1	257.049	15.554	.002
V	770.026	3	256.675	15.532	.000
J	9747.967	4	2436.992	147.465	.000
C * V	47.021	3	15.674	.948	.448
C * J	61.292	4	15.323	.927	.480
V * J	2085.094	12	173.758	10.514	.000
Error	198.311	12	16.526		
Total	45750.309	40			
Corrected Total	13166.762	39			

a. R Squared = .985 (Adjusted R Squared = .951)

Table 3.10 Duncan test result of electrolyte flow rate (*V*) for $NaNO_3$ electrolyte

Duncan[a,b]

V	N	Subset 1	Subset 2
500	10	23.2040	
1000	10	25.2260	
1600	10		32.6420
2500	10		33.0920
Sig.		.288	.809

Means for groups in homogeneous subsets are displayed.
Based on Type II Sum of Squares
The error term is Mean Square(Error) = 16.526.

a. Uses Harmonic Mean Sample Size = 10.000.

b. Alpha = .05.

Table 3.11 Duncan test result of current density (J) for $NaNO_3$ electrolyte

Duncan[a,b]

J	N	Subset 1	2	3	4
6.4	8	10.8212			
3.2	8		15.2887		
12.8	8			22.4913	
25.6	8				45.1838
51.2	8				48.9200
Sig.		1.000	1.000	1.000	.091

Means for groups in homogeneous subsets are displayed.
Based on Type II Sum of Squares
The error term is Mean Square(Error) = 16.526.

a. Uses Harmonic Mean Sample Size = 8.000.

b. Alpha = .05.

Fig. 3.13 Plots of current efficiency (Y) and variables of electrolyte concentration (C), electrolyte flow rate (V), and current density (J) for $NaNO_3$ electrolyte

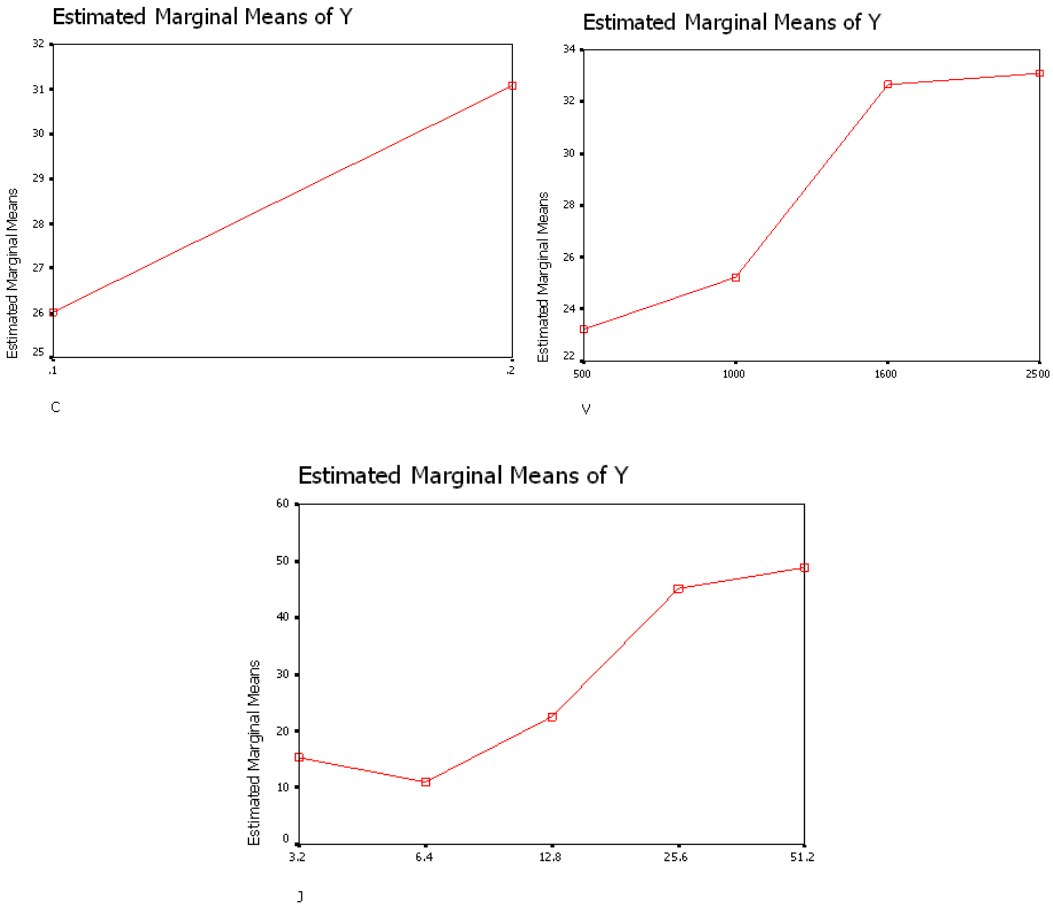

Fig. 3.14 Plots of current efficiency (Y) and two-way terms for $NaNO_3$ electrolyte

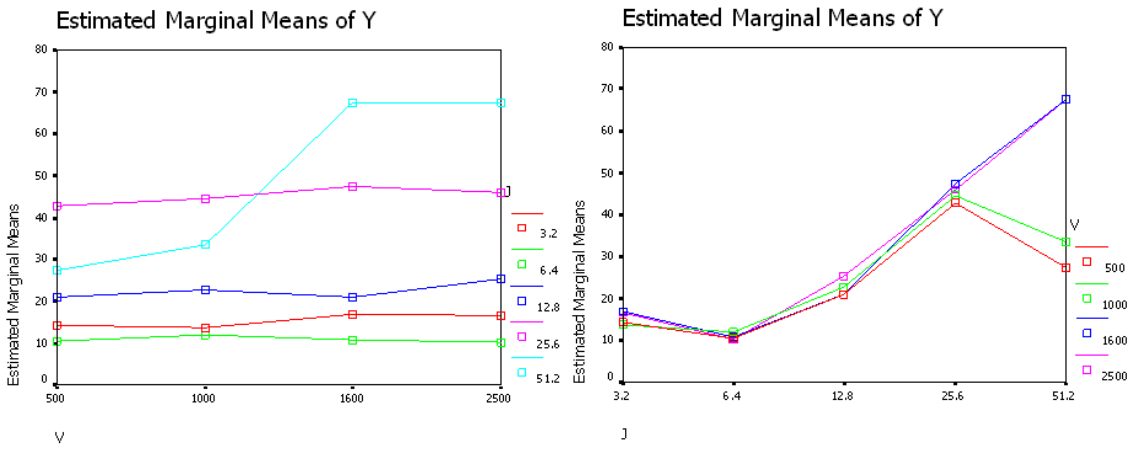

The graphs of the means for the five levels of current density are not parallel, and the graphs of the means for the four levels of flow rate are also not parallel in the plots in figure 3.14, implying that the interactions would be considered important interactions.

Linear Regression Analysis

For the stepwise linear regression for this study all of the variables included in the ANOVA model and the squared values of *C, V*, and *J* were included as potential variables.

The results of the stepwise regression analysis are shown in table 3.12 with the final model having two significant parameters including two-way interaction terms *C*J* and *V*J*. The results indicate that the interrelationships among the variables have stronger influence on the current efficiency than any of the single dependent parameters. The

relation between current density and current efficiency can vary in electrolyte concentration and flow rate. This model is given by:

$$\eta = 12.681 + 1.961C^{*}J + 3.609 \times 10^{-4} V^{*}J \quad (3.6)$$

Table 3.12 Regression results from SPSS for $NaNO_3$ electrolyte

Model Summary[c]

Model	R	R Square	Adjusted R Square	Std. Error of the Estimate
1	.845[a]	.713	.706	9.96382
2	.875[b]	.765	.753	9.13704

a. Predictors: (Constant), VJ

b. Predictors: (Constant), VJ, CJ

c. Dependent Variable: Y

ANOVA[c]

Model		Sum of Squares	df	Mean Square	F	Sig.
1	Regression	9394.210	1	9394.210	94.626	.000[a]
	Residual	3772.552	38	99.278		
	Total	13166.762	39			
2	Regression	10077.798	2	5038.899	60.357	.000[b]
	Residual	3088.964	37	83.486		
	Total	13166.762	39			

a. Predictors: (Constant), VJ

b. Predictors: (Constant), VJ, CJ

c. Dependent Variable: Y

Table 3.13 Linear regression models and excluded variables result for $NaNO_3$ electrolyte

Coefficients[a]

Model		Unstandardized Coefficients		Standardized Coefficients	t	Sig.
		B	Std. Error	Beta		
1	(Constant)	14.977	2.104		7.119	.000
	VJ	4.883E-04	.000	.845	9.728	.000
2	(Constant)	12.681	2.090		6.069	.000
	VJ	3.609E-04	.000	.624	5.635	.000
	CJ	1.961	.685	.317	2.861	.007

Excluded Variables[c]

Model		Beta In	t	Sig.	Partial Correlation	Collinearity Statistics Tolerance
1	C	.140[a]	1.645	.108	.261	1.000
	V	-.227[a]	-2.454	.019	-.374	.778
	J	.312[a]	2.391	.022	.366	.394
	CV	-.090[a]	-.955	.346	-.155	.852
	CJ	.317[a]	2.861	.007	.426	.517
	CC	.140[a]	1.645	.108	.261	1.000
	VV	-.237[a]	-2.592	.014	-.392	.786
	JJ	.131[a]	.980	.334	.159	.424
2	C	.042[b]	.458	.650	.076	.779
	V	-.128[b]	-1.220	.231	-.199	.571
	J	.074[b]	.362	.720	.060	.155
	CV	-.056[b]	-.638	.528	-.106	.835
	CC	.042[b]	.458	.650	.076	.779
	VV	-.144[b]	-1.399	.171	-.227	.586
	JJ	-.269[b]	-1.526	.136	-.246	.198

a. Predictors in the Model: (Constant), VJ

b. Predictors in the Model: (Constant), VJ, CJ

c. Dependent Variable: Y

3.5.3 Statistical Analysis of Current Efficiency with Electrolyte of $NaNO_3$ and Citric acid

This analysis was done on two levels of concentration (*C*), four levels of electrolyte flow rate (*V*), and five levels of current density (*J*). Electrolyte concentration (*C*) levels were 10% and 20%. The electrolyte flow rate (*V*) levels were 500ml/min, 1000ml/min, 1600ml/min, and 2500ml/min. The five levels of current density (*J*) were 3.2A/cm^2, 6.4/cm^2, 12.8A/cm^2, 25.6A/cm^2, and 51.2A/cm^2. The citric acid concentration is 10% by weight and stays constant.

ANOVA

The initial model that was investigated in the general form of the three factor analysis of variance (ANOVA) model for this study was:

$$\eta=\mu+C+V+J+C*V+C*J+V*J+\varepsilon \qquad (3.5)$$

The ANOVA results are shown in table 3.14 along with the results of the Duncan Multiple Range tests for *V* and *J*. The results show that *C, V, J, V*J* and *C*J* were significant. The Duncan tests showed two groupings for the V levels and that all levels of J differed significantly. The two interaction graph pairs indicate that the interactions are not just significant but important.

Table 3.14 ANOVA results for electrolyte of $NaNO_3$ and Citric acid

Tests of Between-Subjects Effects

Dependent Variable: Y

Source	Type II Sum of Squares	df	Mean Square	F	Sig.
Corrected Model	12782.725[a]	27	473.434	53.339	.000
Intercept	31530.471	1	31530.471	3552.342	.000
C	298.553	1	298.553	33.636	.000
V	429.047	3	143.016	16.113	.000
J	10728.757	4	2682.189	302.186	.000
C * V	41.311	3	13.770	1.551	.252
C * J	90.925	4	22.731	2.561	.093
V * J	1194.131	12	99.511	11.211	.000
Error	106.512	12	8.876		
Total	44419.708	40			
Corrected Total	12889.237	39			

a. R Squared = .992 (Adjusted R Squared = .973)

Table 3.15 Duncan test result of electrolyte flow rate (*V*) for $NaNO_3$ and citric acid electrolyte

Duncan[a,b]

V	N	Subset 1	Subset 2	Subset 3
1000	10	25.0820		
500	10	25.3250		
2500	10		28.7270	
1600	10			33.1700
Sig.		.858	1.000	1.000

Means for groups in homogeneous subsets are displayed.
Based on Type II Sum of Squares
The error term is Mean Square(Error) = 8.876.

a. Uses Harmonic Mean Sample Size = 10.000.

b. Alpha = .05.

Table 3.16 Duncan test result of current density (J) for $NaNO_3$ and citric acid electrolyte

Duncan[a,b]

J	N	Subset 1	2	3	4
6.40	8	10.5825			
3.20	8	13.4675			
12.80	8		21.3913		
25.60	8			43.9500	
51.20	8				50.9887
Sig.		.077	1.000	1.000	1.000

Means for groups in homogeneous subsets are displayed.
Based on Type II Sum of Squares
The error term is Mean Square(Error) = 8.876.

a. Uses Harmonic Mean Sample Size = 8.000.

b. Alpha = .05.

Fig. 3.15 Plots of current efficiency (Y) and variables of electrolyte concentration (C), electrolyte flow rate (V), and current density (J) for $NaNO_3$ and citric acid electrolyte

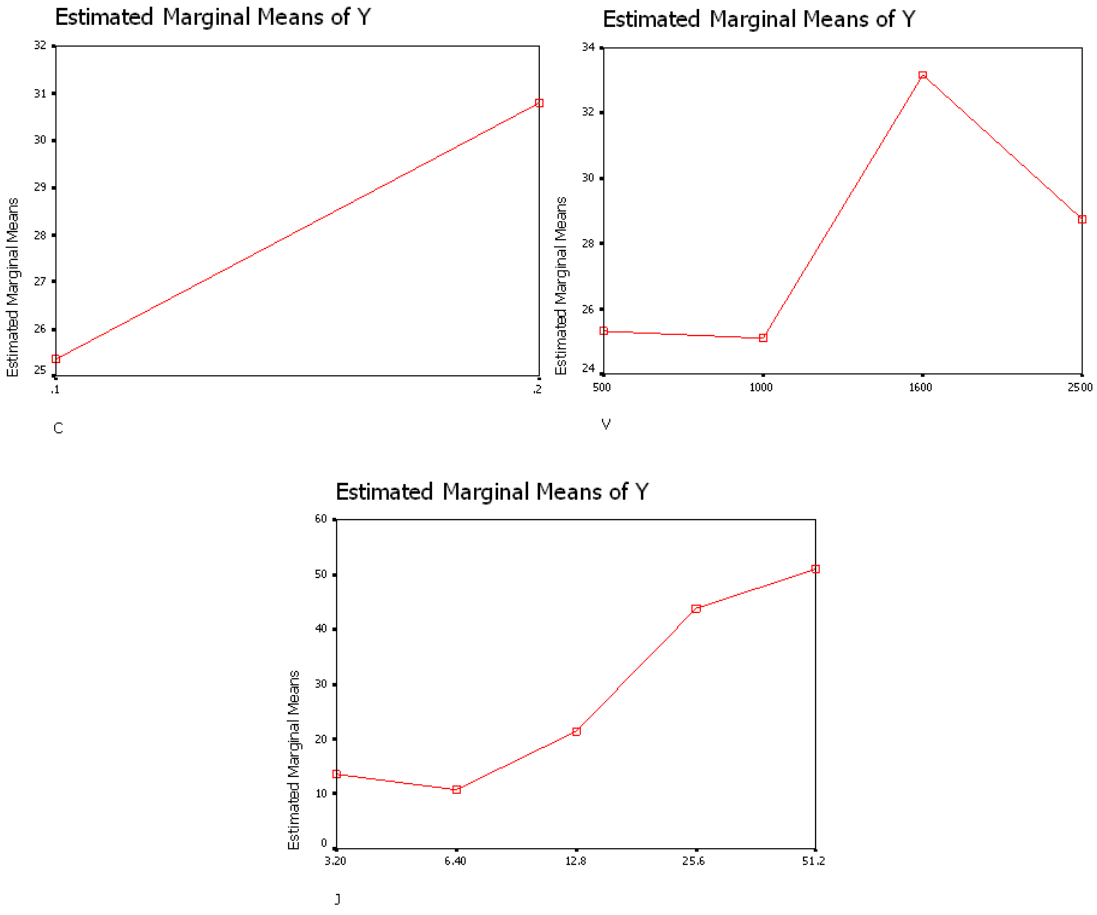

Fig. 3.16 Plots of current efficiency (*Y*) and two-way terms (*V***J* and *C***J*) for $NaNO_3$ and citric acid electrolyte

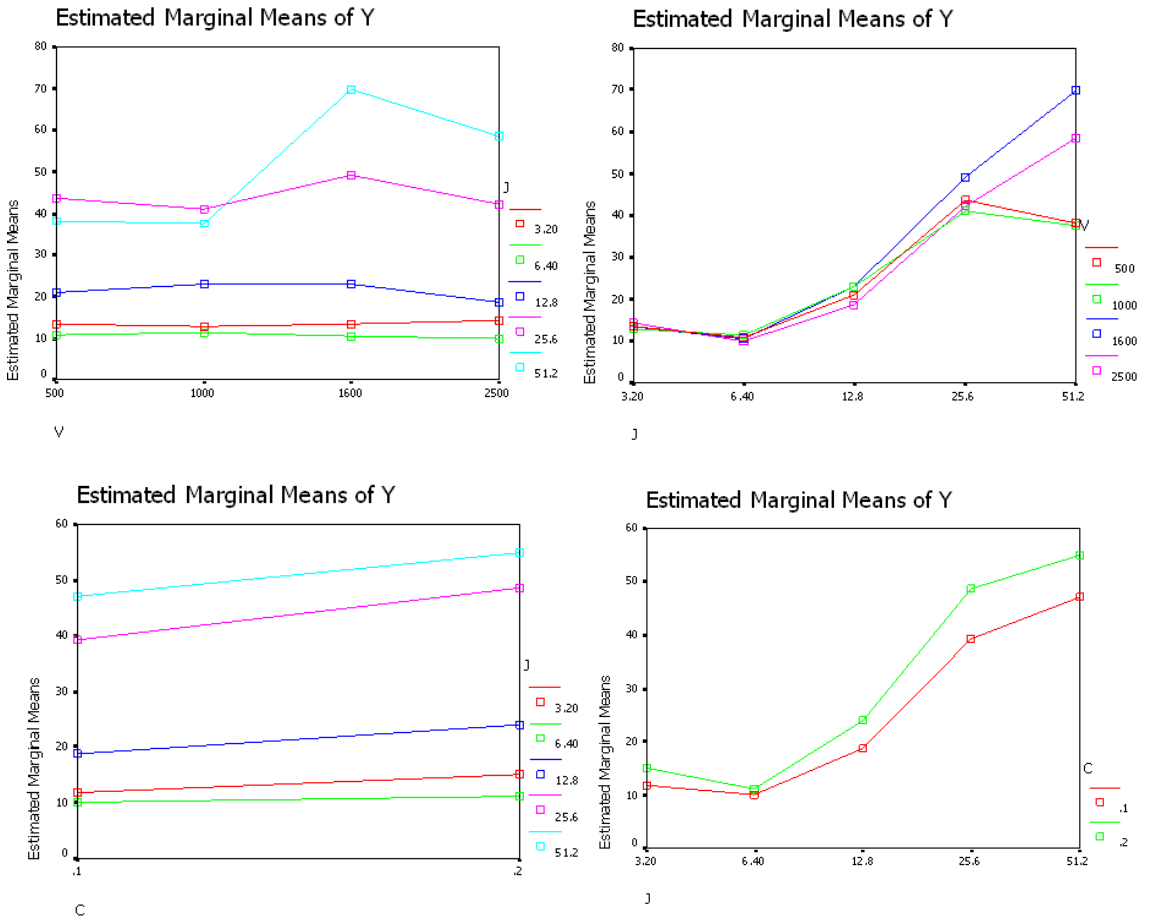

The graphs of the means for the five levels of current density are not parallel, and the graphs of the means for the four levels of flow rate are also not parallel in the first two plots in figure 3.16, implying that the interactions would be considered important interactions. The graphs of the means for the five levels of current density are not parallel, and the graphs of the means for the two levels of electrolyte concentration are

also not parallel in the first two plots in the last two plots in figure 3.16, implying that the interactions would be considered important interactions.

Linear Regression Analysis

For the stepwise linear regression for this study all of the variables included in the ANOVA model and the squared values of *C, V*, and *J* were included as potential variables. The results of the stepwise regression analysis are shown in table 3.17 with the final model having two significant parameters including current density (*J*) and three two-way interaction terms (J^2, *V*J, and C*J*). This model is given by:

$$\eta = 2.394 + 1.451J - 2.091\times 10^{-2} J^2 + 1.883\times 10^{-4} V*J + 2.105C*J \qquad (3.7)$$

Table 3.17 Regression results from SPSS for electrolyte of $NaNO_3$ and Citric acid

Model Summary[e]

Model	R	R Square	Adjusted R Square	Std. Error of the Estimate
1	.852[a]	.726	.719	9.63633
2	.891[b]	.794	.783	8.47750
3	.915[c]	.836	.823	7.65435
4	.928[d]	.860	.844	7.17104

a. Predictors: (Constant), J
b. Predictors: (Constant), J, JJ
c. Predictors: (Constant), J, JJ, VJ
d. Predictors: (Constant), J, JJ, VJ, CJ
e. Dependent Variable: Y

ANOVA[e]

Model		Sum of Squares	df	Mean Square	F	Sig.
1	Regression	9360.600	1	9360.600	100.805	.000[a]
	Residual	3528.637	38	92.859		
	Total	12889.237	39			
2	Regression	10230.121	2	5115.061	71.173	.000[b]
	Residual	2659.116	37	71.868		
	Total	12889.237	39			
3	Regression	10780.028	3	3593.343	61.331	.000[c]
	Residual	2109.208	36	58.589		
	Total	12889.237	39			
4	Regression	11089.402	4	2772.351	53.912	.000[d]
	Residual	1799.834	35	51.424		
	Total	12889.237	39			

a. Predictors: (Constant), J
b. Predictors: (Constant), J, JJ
c. Predictors: (Constant), J, JJ, VJ
d. Predictors: (Constant), J, JJ, VJ, CJ
e. Dependent Variable: Y

Table 3.18 Linear regression models and excluded variables result for electrolyte of $NaNO_3$ and Citric acid

Coefficients[a]

Model		Unstandardized Coefficients		Standardized Coefficients		
		B	Std. Error	Beta	t	Sig.
1	(Constant)	10.690	2.307		4.635	.000
	J	.876	.087	.852	10.040	.000
2	(Constant)	2.394	3.131		.765	.449
	J	2.030	.341	1.974	5.962	.000
	JJ	-2.091E-02	.006	-1.152	-3.478	.001
3	(Constant)	2.394	2.827		.847	.403
	J	1.767	.319	1.718	5.533	.000
	JJ	-2.091E-02	.005	-1.152	-3.852	.000
	VJ	1.883E-04	.000	.329	3.064	.004
4	(Constant)	2.394	2.649		.904	.372
	J	1.451	.326	1.411	4.456	.000
	JJ	-2.091E-02	.005	-1.152	-4.112	.000
	VJ	1.883E-04	.000	.329	3.270	.002
	CJ	2.105	.858	.344	2.453	.019

The results from this statistical analysis can be explained by introducing electrical conductivity. High electrolyte concentration helps increasing electrical conductivity and high current efficiency could be achieved consequently. Sufficient electrolyte flow allows the products of machining to be so readily flushed from the machining gap, thus improve current efficiency.

3.5.4 Comparison of the Models Developed with New Experimental Data

Twenty new data points were collected to verify the adequacy of the models developed. One electrolyte flow rate value was randomly selected as 1600ml/min for this validation. Two levels of concentration (10% and 20%) were used and five levels of current density (3.2A/cm^2, 6.4/cm^2, 12.8A/cm^2, 25.6A/cm^2, and 51.2A/cm^2) were used. These experimental results were obtained by changing the parameter of pulse on-time from 5ms to 15ms. This resulted in 20 new data points.

The results were compared with the values predicted by the models and their associated prediction intervals. The comparisons were done in two ways - compare the profiles of the current efficiency graphically and compare the current efficiency (η) values obtained from actual experiments with the predicted values and their associated prediction intervals obtained from the linear regression models.

Figure 3.17 shows the current efficiency value for $NaNO_3$ electrolyte with the plots of actual experimental values and the model generated values. Figure 3.18 shows the current efficiency value for $NaNO_3$ and citric acid electrolyte with the plots of actual experimental values and the model generated current efficiency values. Both the figures indicate that for all cases, there are small differences between the actual values and the model generated values. However, the differences in figure 3.18 are obviously larger than figure 3.17, which indicates the model for $NaNO_3$ electrolyte may be more accurate than the model for $NaNO_3$ and citric acid electrolyte. That is the indication for this data.

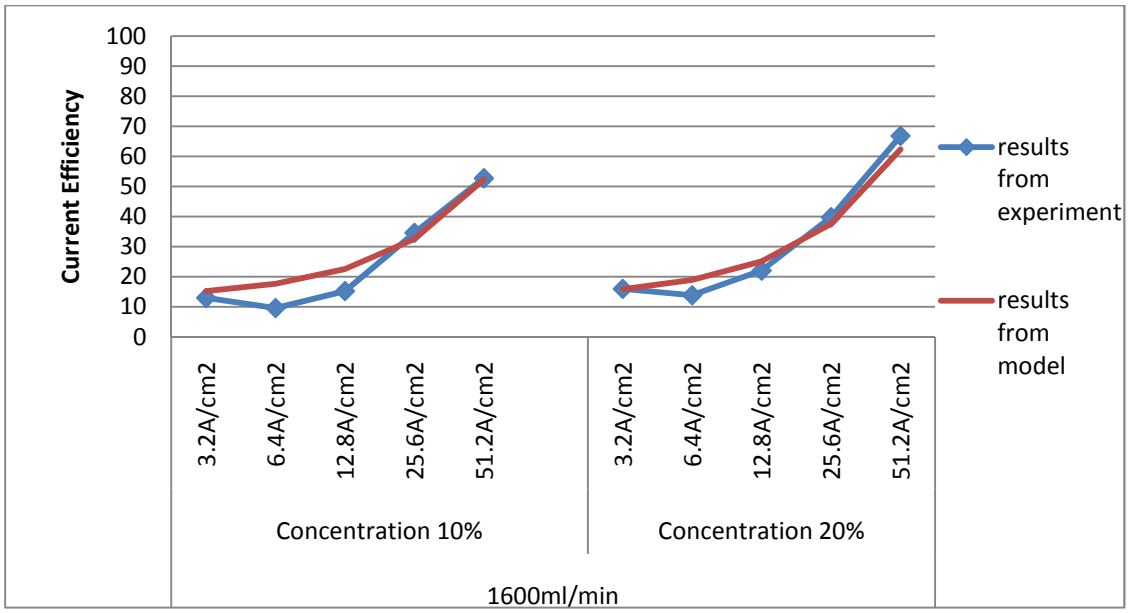

Fig. 3.17 Comparison of current efficiency values of $NaNO_3$ electrolyte

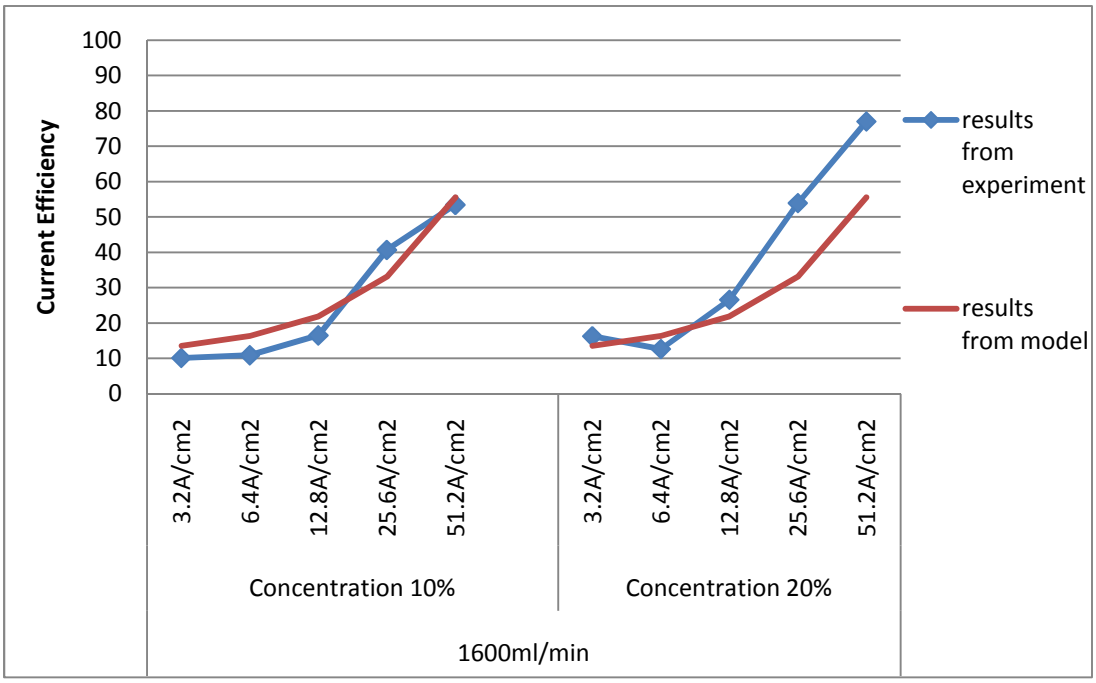

Fig. 3.18 Comparison of current efficiency values of $NaNO_3$ +Citric acid electrolyte

Prediction intervals from the models and experimental results for the two kinds of electrolytes are shown in table 3.19 and table 3.20 separately. It can be seen from table 3.19 that all of the experimental results fell within their corresponding prediction intervals. However, for table 3.20, the last experimental result (in red) doesn't fall within its corresponding prediction interval. A conclusion can be derived that the two linear regression models are basically reliable.

Table 3.19 Comparison of current efficiency values of $NaNO_3$ electrolyte

$NaNO_3$ Electrolyte					
Flow rate 1600ml/min	Parameters Concentration 10%	Current density 3.2A/cm2	results from experiment 12.92	prediction interval from model -3.77755	34.08972
		6.4A/cm2	9.56	-1.25642	36.51926
		12.8A/cm2	15.18	3.74975	41.41441
		25.6A/cm2	34.56	13.61678	51.35004
		51.2A/cm2	52.69	32.78068	71.79147
	20%	3.2A/cm2	15.95	-3.11666	34.68383
		6.4A/cm2	13.81	0.05593	37.71691
		12.8A/cm2	21.98	6.33617	43.848
		25.6A/cm2	39.72	18.63488	56.37197
		51.2A/cm2	66.78	42.22953	82.42267

Table 3.20 Comparison of current efficiency values of $NaNO_3$ +Citric acid electrolyte

$NaNO_3$ and Citric acid Electrolyte					
Flow rate 1600ml/min	Parameters Concentration 10%	Current density 3.2A/cm2	results from experiment 10.14	prediction interval from model -6.63141	23.55376
		6.4A/cm2	10.9	-0.78197	28.9816
		12.8A/cm2	16.5	9.20313	38.98206
		25.6A/cm2	40.68	23.54466	54.33565
		51.2A/cm2	53.45	31.97172	64.19476
	20%	3.2A/cm2	16.25	-5.95789	24.22727
		6.4A/cm2	12.64	0.56507	30.32863
		12.8A/cm2	26.59	11.89721	41.67614
		25.6A/cm2	53.94	28.93281	59.7238
		51.2A/cm2	77.02	42.74803	74.97106

The difference between the regression models and experimental results can be explained. The regression models are based on the theoretical assumption that the independent variable values are exact and can be set without error or variation. This is

probably not absolutely true. Additionally, there is the assumption that the current efficiency is only due to the parameters selected from previous experiments and other influence factors like temperature and pulse on-time are considered as fixed factors. In fact, the pulse on-time was different for the validation data and may explain some of the variation of the actual values from the predicted values. The electrolyte flow rate has an effect on current efficiency through heat generation, pulse on/off –time could also affect current efficiency to a certain extant in a similar way. The parameter values are restricted to a certain range in these experiments for an in-house built electrochemical cell. In statistical analysis, the stepwise regression algorithm allows a variable brought into the model at an earlier stage, to be dropped subsequently if it is no longer helpful in conjunction with variables added at later stages [33].

CHAPTER 4

MODELING AND SIMULATION

4.1 Introduction

This study presents a simulation model for the anodic dissolution process in PECM which takes into consideration the activation and concentration overpotential at electrodes, and diffusion layer on the electrode surface. Most of the previous studies assume insignificant overpotential, negligible oxides formation on electrode surfaces, unimportant electric field effects of the edge at the work cavity, and constant electrolyte conductivity during PECM process [34]. In spite of the reported studies, an investigation into the anodic dissolution process in PECM is needed to explain the effect of the process parameters on current efficiency and to understand the mechanism of pulse electrochemical machining. Experimental studies indicate the validity of the proposed simulation model.

The modeling and simulation starts with the problem statement [35]. PECM is a stochastic process involving complex electrochemical reactions during metal dissolution. The nature of this process makes it difficult to fully understand the process. With simplifying assumptions, any complex process can be separated into simpler processes that yield a mechanism to control the process. In the same way, the process of metal removal in PECM can be categorized into an electrical process (applying the pulse current), a chemical process (chemical reactions), a thermal process (heating of the electrolyte), and a hydrodynamic process (machining products removal). When the pulse current power supply is applied to two electrodes that are submerged in an electrolyte, the

atoms and ions interchange by the addition of electrons from the external circuit. The chemical reactions depend upon the workpiece material and the electrolyte type. The external power supply accelerates the chemical reactions by providing extra electrons. The anodic electrochemical dissolution occurs during the pulse on-times and the electrolyte is heated up by converting electrical work into heat. The flowing electrolyte flushes away dissolution products (sludge, gas bubbles and heat) from the interelectrode gap during the pulse off-times. In PECM process, the accumulation of machining products hinders the further machining. To remove these products, pulse current and flowing electrolyte could induce electrolyte turbulence and thus increase electrolyte conductivity.

4.2 Current Density Expression and Electrode Potential Estimation

4.2.1 Pulse Current

This section discusses about the non- sinusoidal periodic pulse current (figure 4.1). Fourier series was used to form the pulse current equation in terms of the harmonics.

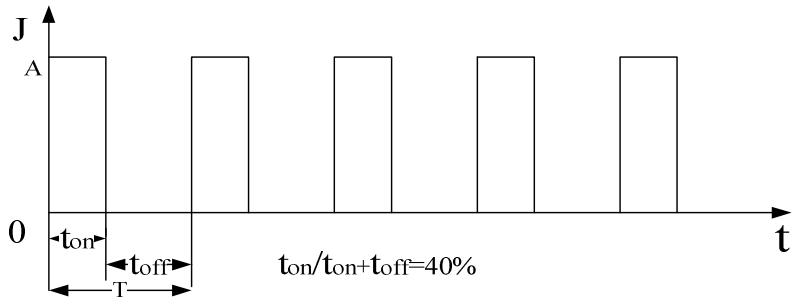

Fig. 4.1 Non- sinusoidal periodic pulse current with pulse on-time (t_{on}) and pulse off-time (t_{off})

The current density J as a function of time t is given by [36, 37]

$$J(t) = \begin{cases} J_p \ (0 \le t \le \frac{2T}{5}) \\ J_b \ (\frac{2T}{5} < t < T) \end{cases} = \begin{cases} A \ (0 \le t \le \frac{2T}{5}) \\ 0 \ (\frac{2T}{5} < t < T) \end{cases} \quad (4.1)$$

$and,\ J_p = [J \cdot (1 + \frac{t_{on}}{t_{off}}) - J_b]$

where,

J_p is the peak current density

$\frac{t_{on}}{t_{off}}$ is the ratio of pulse on-time and pulse off-time

J_b is the base current density

If the function $J(t)$ has period of 2π , then its Fourier series is [36, 37]

$$J(t) = a_0 + \sum_{k=1}^{\infty}(a_k \cos k\omega t + b_k \sin k\omega t) = A_0 + \sum_{k=1}^{\infty} A_{km} \sin(k\omega t + \varphi_k) \quad (4.2)$$

with Fourier coefficients defined by the integrals [36, 37]

$$a_0 = \frac{1}{2\pi}\int_0^{2\pi} J(t) d(\omega t)$$

$$a_k = \frac{1}{\pi}\int_0^{2\pi} J(t) \cos k\omega t \, d(\omega t)$$

$$b_k = \frac{1}{\pi}\int_0^{2\pi} J(t) \sin k\omega t \, d(\omega t)$$

$$A_0 = a_0$$

$A_{km} = \sqrt{a_k^2 + b_k^2}$, $a_k = A_{km} \sin \varphi_k$, $b_k = A_{km} \cos \varphi_k$

$$\varphi_k = arc \tan \frac{a_k}{b_k}$$

The constants $A_{0,}$ A_{km}, and φ_k for the non- sinusoidal periodic pulse current (figure 4.2) are

$$A_0 = \frac{A}{2.5}$$

$$A_{km} = \frac{A}{k\pi}\sqrt{-2(\cos(0.8k\pi) - 1)}$$

$$\varphi_k = \ arc\tan\frac{\frac{A}{k\pi}\sin(0.8k\pi)}{\frac{A}{k\pi}[1 - \cos(0.8k\pi)}$$

Thus, the Fourier series is given by

$$J(t) = \frac{A}{2.5} + \sum_{k=1}^{\infty}\frac{A}{k\pi}\sqrt{-2(\cos(0.8k\pi) - 1)}\sin(k\omega t + arc\tan\frac{\sin(0.8k\pi)}{[1-\cos(0.8k\pi)]}) \quad (4.3)$$

$and,\ \frac{A}{2.5}$ is the direct current component

A_{1m} is the amplitude of the fundamental harmonic $(k = 1)$

A_{2m} is the amplitude of the second harmonic $(k = 2)$

Figure 4.2 shows the direct current, the fundamental harmonic, and the second harmonic of the Fourier series for current density. In this case, the current density can now be rewritten omitting the third and higher harmonic as

$$J(t) = \frac{A}{2.5} + 0.61A\cos(t) + 0.19A\sin(\frac{t-90^{\circ}}{3}) \quad (4.4)$$

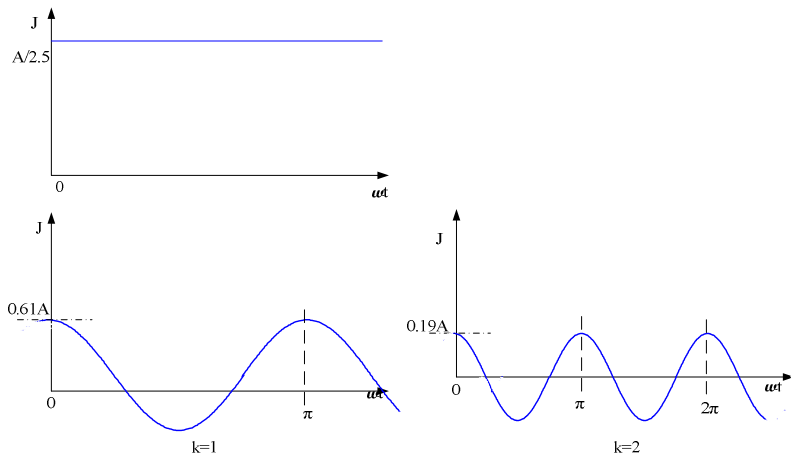

Fig. 4.2 Part of the Fourier series for the square wave function

4.2.2 Electrode Potential

In this section, the electrolyte concentration, thickness of diffusion layer, and the diffusion coefficient were considered as constants to get the equations for actual potentials at anode and cathode. The actual potentials can be expressed as [1]

$E = \eta_{(activation)} + \eta_{(concentration)}$, at the cathode (4.5)

$E = E_{(applied)} - [\eta_{(activation)} + \eta_{(concentration)}]$, at the anode (4.6)

where,

$\eta_{(activation)}$ is the activation overpotential

$\eta_{(concentration)}$ is the concentration overpotential

The activation overpotential and concentration overpotential are given by [1]

$$\eta_{(activation)} = \frac{2.303\mathrm{RT}}{\mathrm{zaF}} \log \mathrm{J}_0 + \frac{2.303\mathrm{RT}}{\mathrm{zaF}} log(J_{(t)}) \quad (4.7)$$

$$\eta_{(concentration)} = -\frac{kT}{e} ln\left(1 + \frac{\delta_0 (\frac{D}{\nu})^{1/3} \cdot J_{(t)}}{e C_\delta D_m}\right) \quad (4.8)$$

where,

$J_0 \cong 10^{-5}$A/cm^2, and $a \cong 1/2$

k is Boltzmann's constant ($1.380\,6504(24) \times 10^{-23}$ J K^{-1})

R is the universal gas constant (8.314JK^{-1} mol^{-1})

C_δ is the value of the bulk concentration of the electrolyte,

C is the thickness of δ depends on the electrolyte flow conditions

D is the diffusion coefficient, which depends on concentration and temperature, and assumed constant, $D \cong 10^{-5}$cm^2/s

u is the ionic mobility

e is the electronic charge ($1.6\times 10^{-19}\ C$)

U is the local solution velocity, assume U=0

δ_0 is the hydrodynamic, laminar boundary layer thickness

v is the kinematic viscosity of the solution, $v\cong 10^{-3}\text{cm}^2/\text{s}$

Substituting equations (4.7) & (4.8) into (4.5) & (4.6) separately we get

$$E= 0.5 - 0.03\log(J_{(t)}) - 0.025\ln[1 + (1.7\times 10^{21})J_{(t)}],\ \text{at the cathode} \quad (4.9)$$

$$E=9.5+0.03\log(J_{(t)}) + 0.025\ln[1 + (1.7\times 10^{21})J_{(t)}]\ ,\ \text{at the anode} \quad (4.10)$$

where,

$J_{(t)}$ is the current density with function of time

4.3 Analysis of the Anodic Dissolution Process

4.3.1 Chemical Reactions and Model Assumptions

The physical model for the machining products removal is shown in the figure 4.3. The heat transfer is through convection and conduction. The momentum transport is treated as a turbulent flow, which is built on a Reynolds average formulation of Navier-Stokes equations. The Nernst-Planck application mode is applied to predict the transport and reaction, which are caused by the **c**onvection, diffusion, and migration in the electro neutrality condition. We are assuming the reactions take place at the anode and the cathode are nickel dissolution and hydrogen evolution. Only the reactions that take place close to the electrodes are considered. The chemical reaction equations and their corresponding standard electrode potential are [38]

$Ni - 2e^- \rightarrow Ni^{2+}$ $(-0.25\ V)$, at the anode

$2H^+ + 2e^- \rightarrow H_2 \uparrow (-0.42\ V)$, at the cathode

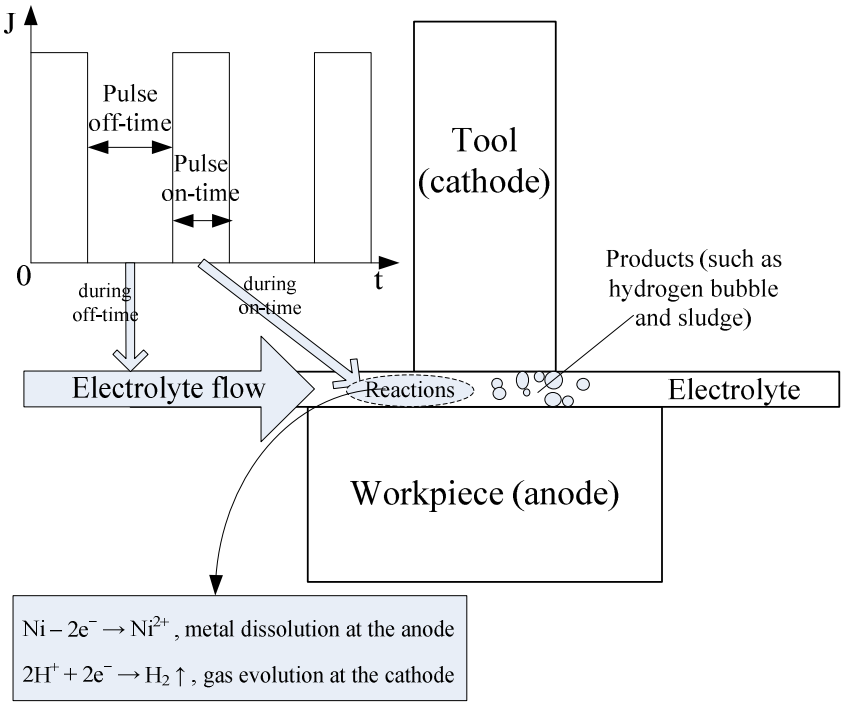

Fig. 4.3 Physical model of products removal

In this study, Faraday's law is employed to theoretically analyze the PECM process. The analysis is based on the following assumptions:

1. the material valence is identified before processing;
2. only activation overpotential and concentration overpotential are considered;
3. the non-sinusoidal periodic pulse current is approximately equal to the sum of the direct current component, the fundamental harmonic, and the second harmonic;
4. the metal is only removed by the dissolution, that is, collapse does not happen. The processed material is dissolved at the atomic level, and the atoms do not exfoliate and cluster in a group.

4.3.2 Modeling Procedures

In order to build up the anodic dissolution process simulation model, the current efficiency behavior needs to be parameterized at first. This required conducting experiments using the in-house designed PECM setup. The experimental results obtained from the third set of experiments are shown in Appendix A4. The results of the stepwise regression analysis from chapter three indicate that the interrelationships among the variables have stronger influence on the current efficiency than any of the single dependent parameters. The relation between current density and current efficiency can vary in electrolyte concentration and flow rate. This model is given by the equation (3.6).

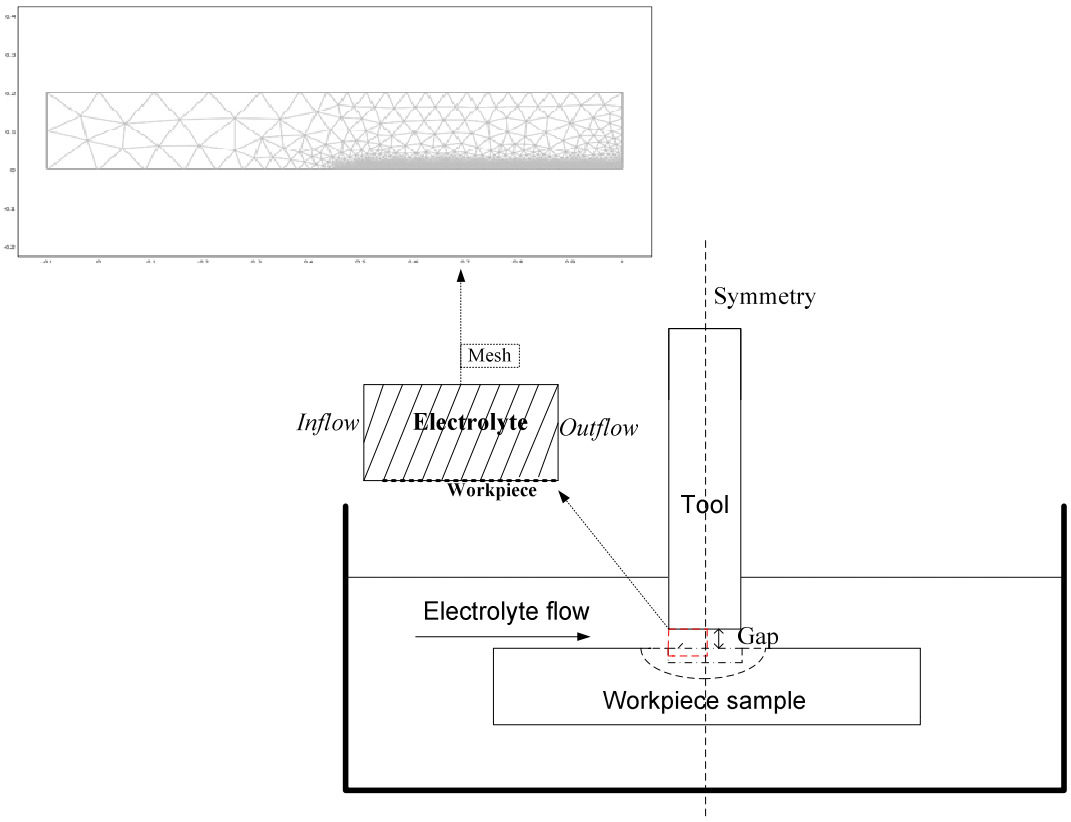

Fig 4.4 Meshed geometry of modeled device

The PECM model comprises several physical domains: energy transport by conduction and convection, Navier-Stokes flow description, and mass transport. All the physical domains are linked by process variables being solved simultaneously. Figure 4.4 indicates the meshed geometry of the modeled PECM cell, which has meshed points of 1626, and depicts the electrolyte flow direction and workpiece positions. Table 4.1 shows the parameters used in this model.

Table 4.1 Parameters used in the COMSOL Multiphysics model

Constant	**Value**
Faraday's constant (F)	*96485 C/mol*
Universal gas constant (R)	*8.314J/K·mol*
Boltzmann's constant (k)	1.38×10^{-23} J/K
Electrochemical coefficient(κ)	$2.62\times 10^{-4} g/amp{\cdot}s$
Initial temperature (T_0)	*298K*
Specific heat of the electrolyte(c_e)	*4.2J/K·g*
Thermal conductivity electrolyte (T_C)	*0.6 W/(m·K)*
Electrode length (x)	*1cm*
Current density ($J(t)$)	$\frac{A}{2.5} + 0.61A\cos(t) + 0.19A\sin(\frac{t-90^{\circ}}{3})$

The mathematical description is started with the governing equations and boundary equations. Since we have assumed that heat transfer was through convection and conduction in the energy transport mode we start with it.

Energy transport

The model is described by an energy transport equation with both convection and conduction; see equation 4.11. In these equations, T is the temperature (K), u is the velocity (m/s), ρ represents density (kg/m3), k equals the thermal conductivity (W/(m·K)), and C_p is the heat capacity (J/(kg·K)) [39].

$$\rho C_p u \cdot \nabla T - \nabla \cdot (k \nabla T) = 0 \tag{4.11}$$

The boundary conditions for the problem are: 1) set the inlet temperature to 298 K; 2) at the outlet, apply convective flux as a boundary condition. It assumes that heat transport is dominated by convection and follows form $n \cdot (k \nabla T) = 0$; 3) at all other boundaries, insulating conditions apply: $n \cdot \left(-k \nabla T + \rho C_p T u\right) = 0$

Momentum transport

The model is described by Navier-Stokes equations with both convection and conduction, see equation 4.12. In these equations, η denotes the viscosity of the solution (kg/ (m·s)), u is the velocity (m/s), ρ represents density (kg/m3), p is the pressure (Pa) [39].

$$\rho(u \cdot \nabla)u = \nabla \cdot \left[-pI + \eta(\nabla u + (\nabla u)^T) - \left(\frac{2\eta}{3}\right)(\nabla \cdot u)I\right] + \rho \boldsymbol{g}$$

$$\nabla \cdot (\rho u) = 0 \tag{4.12}$$

The boundary conditions for the problem are: 1) $k-\varepsilon$ equations in the fluid domain; 2) specified velocity at the inlet; 3) specified pressure at the outlet, the viscous stress is assumed to be zero, and the pressure is set according to the atmospheric conditions: $p = 10^5 P_a$

Mass transport

This mass transport mode was conducted in a one dimensional condition. The computational domain is the distance away from workpiece. The governing and boundary equations are given as [39]

$$\nabla \cdot [F \sum_i z_i \left(-D_i \nabla C_i - z_i u_{mi} F C_i \nabla V\right)] = F \sum_i z_i R_i \tag{4.13}$$

$$-n \cdot F \sum_i z_i \left(-D_i \nabla C_i - z_i u_{mi} F C_i \nabla V\right) = i_0 \tag{4.14}$$

In the above equations, C_i is the concentration (mol/m^3), D_i give the diffusivities (m^2/s), z_i equals the charge, u_{mi} represents the mobility ((mol·m^2)/ (J· s)), and R_i is the production term for species i (mol/ (m^3·s)), F denotes Faraday's constant (C/mol), and V is the potential (V). The mobility, u_{mi} can be expressed in terms of D_i, R, and T as $u_{mi} = \frac{D_i}{RT}$. The species considered in the model are the protons, nickel, sodium and hydrogen. This simplified model considers only a one dimensional model of the transport between two electrodes. At the electrode surface specified the fluxes for the ionic species that are included in the electrode reactions, $H^+ and\ Ni^{2+}$. For the inert ionic species, Na^+, the transport through the electrode surface equals zero.

The anodic dissolution simulation results greatly support and minimize experimental effort but cannot eliminate actual experiments. Based on the parameterized

current efficiency behavior that discussed at the beginning of section 4.3.2, the current efficiency fit model is given by

$$\eta = 12.681 + 1.961 C_i * J_{(t)} + 3.609 \times 10^{-4}\, u * J_{(t)} \quad (4.15)$$

In the above equation, $J_{(t)}$ is the current density with function of time, u is the velocity (m/s) from the momentum transport equation (4.12), C_i is the concentration (mol/m^3) from the mass transport equations (4.13) & (4.14). T is the temperature (K) from the energy transport equation (4.11). This variable is also a component of momentum transport and mass transport equations, which connects all the three modules. Equations (4.11-4.15) are solved in the COMSOL Multiphysics equation-based modeling solver under the assumptions that discussed in section 4.3.1.

4.3.3 Multiphysics Simulation Results and Discussion

Figure 4.5 shows the results of simulation at t = 60 s, showing the electrolyte total temperature distribution with the x-axis of electrolyte flow direction. The small electrolyte total temperature increase could have been caused by the electrolyte flow rate raise. At the upper part of electrolyte, convective heat flux is high and able to remove the heat; therefore, temperature increase is small. At the lower edge, the surface of the workpiece, convective flux is not able to remove the heat; therefore, temperature increase at the edge is the highest. Figure 4.6 shows the electrolyte temperature gradient in a greater detail at the surface of the workpiece.

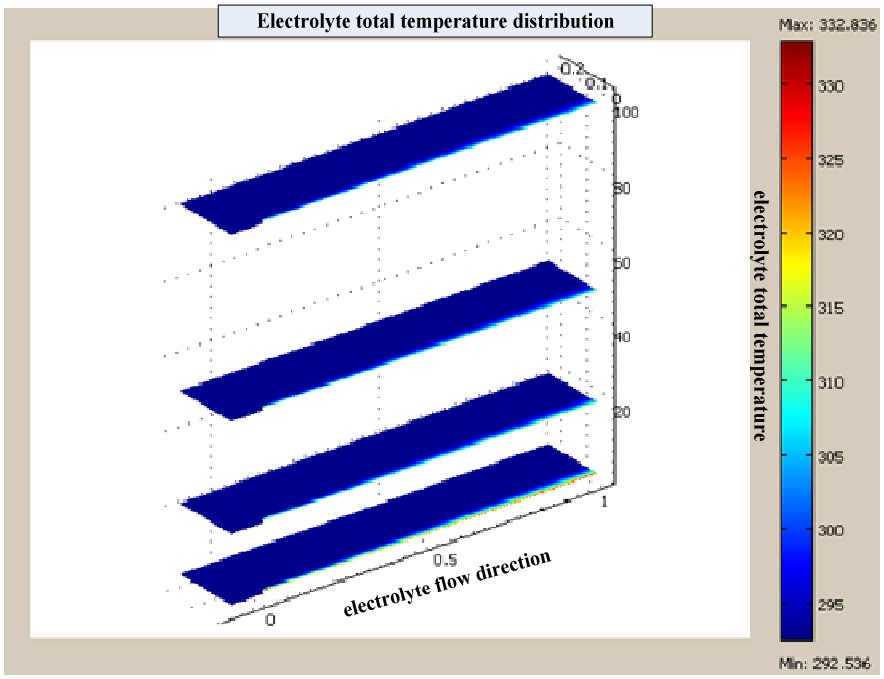

Fig. 4.5 Electrolyte Temperature (K) at different flow rates (Z axis)

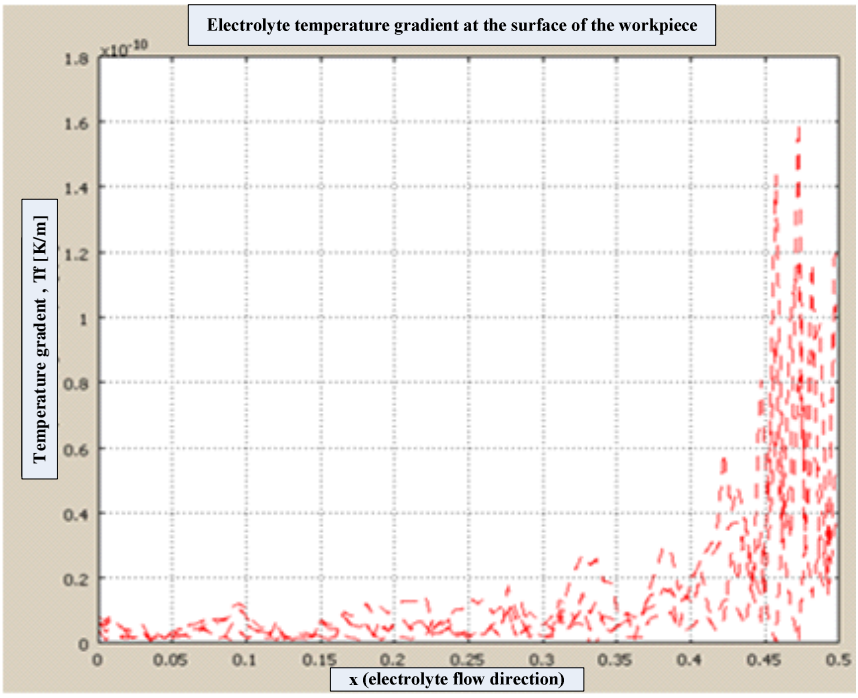

Fig. 4.6 Electrolyte temperature gradient

Figure 4.7 shows the results of simulation at t = 60 s, showing the electrolyte velocity field at the surface of the workpiece. Figure 4.8 shows the electrolyte velocity field at different flow rates in a greater detail at the surface of the workpiece. The viscosity and resistance of electrolyte decrease could have been caused by temperature raise; therefore, the electrolyte velocity could be increased.

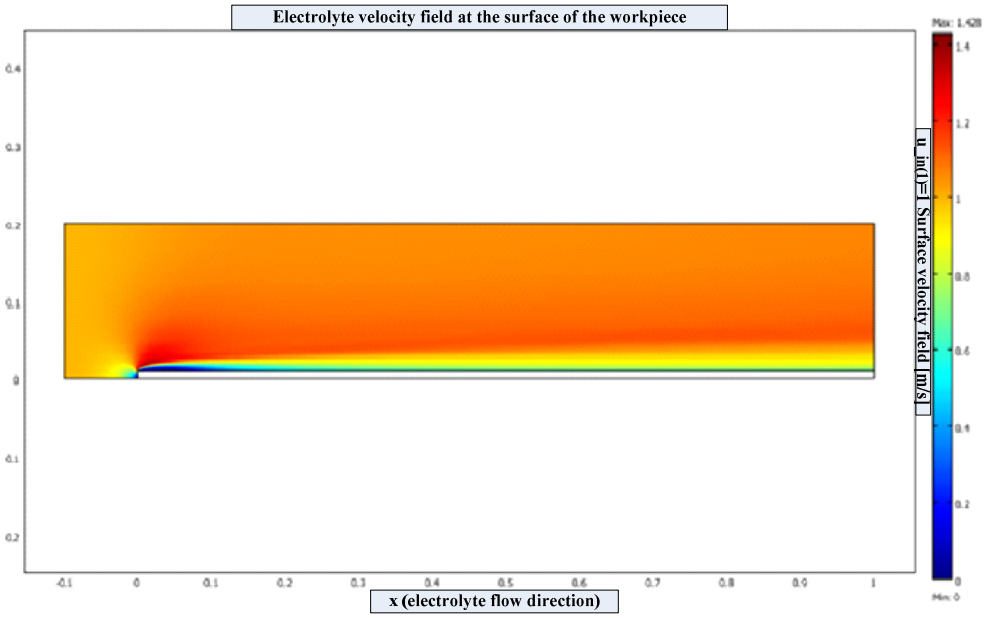

Fig. 4.7 Electrolyte velocity field

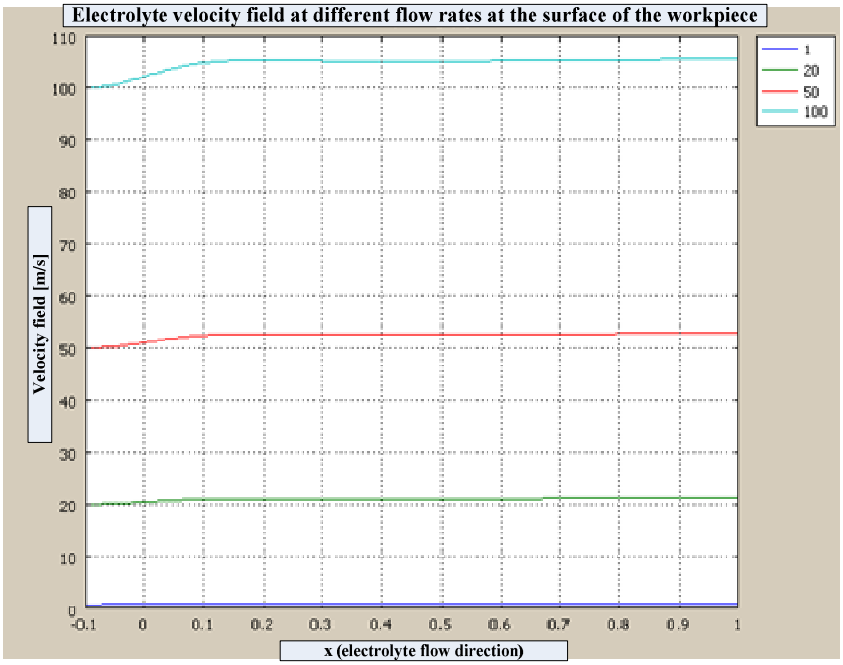

Fig. 4.8 Electrolyte velocity field at different flow rates

Figure 4.9 shows the proton concentration at different time steps (sec) and the x-axis is the distance from workpiece. This result takes place because the current density is not constant over time. At high current densities, large amounts of protons are produced, and this front moves outside in the domain. As the current density is lowered (almost zero), few protons are produced, and this front moves inwards in the domain.

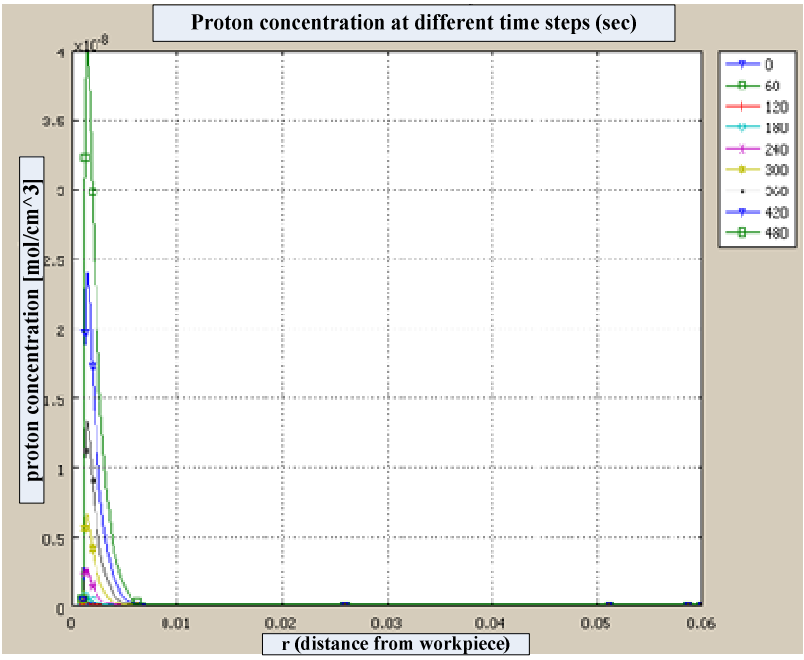

Fig. 4.9 Proton concentration at different time steps

Fig. 4.10 Dimensionless wall offset for various inlet velocities

Figure 4.10 indicates the software's limitation. The mesh is too coarse for this case. Consequently, both the fluid velocity at the boundary and the heat transfer coefficient may become less accurate. Making the mesh finer at the boundary can help correcting this condition but computer memory is exceeded.

4.4 Experimental Verification

The results obtained from the anodic dissolution process simulation model have been verified by experimental results. The experiments were performed on the in-house designed PECM setup. The machine time was set to 1 min, 2 min, 3 min, 4 min, 5 min, 6 min, 7 min, and 8 min. The technical data for the pulse power supply are: pulse on-time $t_{on} = 15ms$, pulse off-time $t_{off} = 22.5ms$. Ten mass percent of sodium nitrate was used as the electrolyte. The electrolyte flow rate was set to 500ml/min. The current efficiency fit model (4.15) provides necessary parametric depiction of current efficiency function and, therefore, for the model simulation.

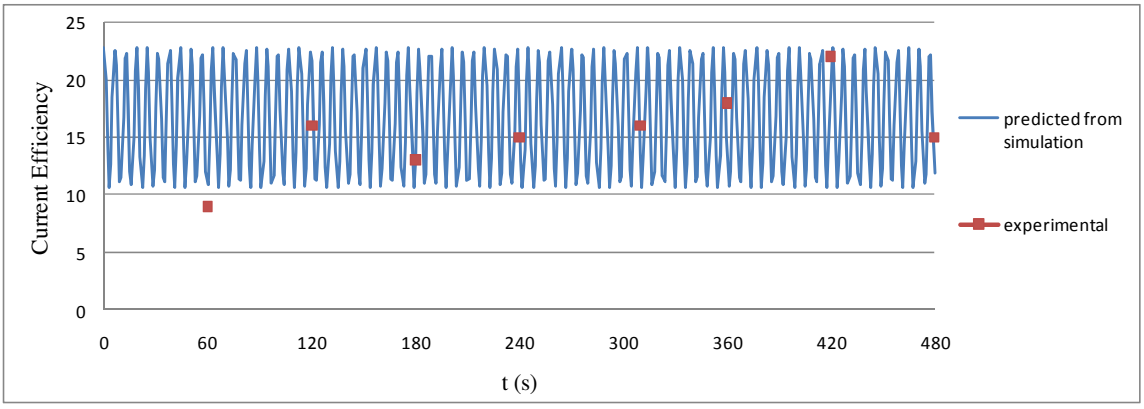

Fig. 4.11 Experimental (red) and simulated (blue) current efficiency

Figure 4.11 shows current efficiency predicted by simulation compared to experimental results. The most obvious difference between the experimental results and simulation results occurs when machine time t (s) is relatively short. This is possible due to the more important effects of gas generation on electrical conductivity in reality than in the simulation model. The predominant effect of gas generation results in low electrical conductivity. When machine time increases, the electrical conductivity drop caused by gas generation decelerates. Thus, the difference between experimental results and simulation results becomes smaller gradually. These differences between the experimental results and simulation results indicate the complexity of electrochemical reactions is more than expected. The study on current efficiency can be broadened by introducing quantum theory.

4.5 Current Density Expression in Quantum Theory

Quantum theory in electrochemistry is the application of quantum mechanical tools to the study of electrochemical processes, including electron and mass transfer at electrodes. The electrical field and mass transport between electrodes determine the current density distribution. The current flowing through the electrolyte is as a result of the motion of ions. Current density can be expressed by applying quantum theory [40].

$$J=e \iint c(x)P_{act}(x,E)\ P_T(x,E)f(E)\rho(E)\,dx\,dE \tag{4.16}$$

where

e is the electronic charge

$c(x)$is the ion concentration

$P_{act}(x, E)$ is ion with E energy appearance probability

$P_T(x, E)$ is the Tunnel probability of electron with E energy in metal electrode

$f(E)$ is the metal electron Fermi distribution function

$\rho(E)$ is the electron state density

As current density mainly depends on activated ions nearest to the electrode surface (the distance is $'\delta'$ and $'\delta'$ is constant for a certain reaction), when ρ(E) equals to $E^{1/2}$, formula (4.16) would turn into formula (4.17) [41]:

$$J = 2e\delta c(1/\pi)^{1/2}(\kappa T)^{-3/2} \int E^{1/2} f(E) P_T(E) P_{act}(E)\, dE \qquad (4.17)$$

where

$P_{act}(E)$ is ion with E energy appearance probability

$P_T(E)$ is the Tunnel probability of electron with E energy in metal electrode

δ is the distance between the center of the ion and the electrode surface

4.5.1 Modification

This section discusses the modification of current density expression in formula 4.17. There are more than one chemical reactions happening in the PECM process and the distance between the center of the ion and the electrode surface would be variable. Therefore, the current density expression can be modified by introducing the probability of finding particles with different $'\delta'$ (the distance between the center of the ion and the electrode surface), given as

$$J=\sum_1^n \rho_n 2e\delta c(1/\pi)^{1/2}(\kappa T)^{-3/2}\int E^{1/2} f(E)P_T(E)P_{act}(E)\,dE \quad (4.18)$$

where

n is the number of particles with different δ (*n=2, 3,4 …*)

ρ_n is the probability of finding particle with $'\delta_n'$ distance between the center of the ion and the electrode surface

4.5.2 Verification

This section would verify the rationality of introducing the concept of $'\rho_n'$ (probability of finding particles with different $'\delta'$ distance between the center of the ion and the electrode surface) from last section. Assume two types of particles exist near to electrode surface with different $'\delta'$ (δ_1 and δ_2) in a three dimensional environment. Assume δ_2 equals to $\frac{1}{2}\delta_1$, and the probability of finding particle with δ_1 distance is one. Then the probability of finding particle with δ_2 distance could be:

For one dimensional case, set $\frac{-a}{2} < \delta_1 < \frac{a}{2}$, by applying the Schrodinger equation and boundary condition: Schrodinger Equation: $-\frac{\hbar^2}{2m}\frac{d^2\varphi}{d{\delta_1}^2}=E\varphi$ [42], for $\frac{-a}{2} < \delta_1 < \frac{a}{2}$, Boundary condition: $\varphi(\frac{a}{2}) = \varphi(-\frac{a}{2}) = 0$, let $\kappa=\sqrt{\frac{2mE}{\hbar^2}}$ and apply general solution, which is: $\varphi(\delta_1)=A\sin(\kappa\delta_1)+B\cos(\kappa\delta_1)$. By boundary condition and normalization condition [42]: $\kappa=\frac{n\pi}{a}$, n=1, 2, 3…, $\varphi_n(\delta_1) = \sqrt{\frac{2}{a}}\cos\frac{n\pi}{a}\delta_1$, n— odd; $\varphi_n(\delta_1) = \sqrt{\frac{2}{a}}\sin\frac{n\pi}{a}\delta_1$, n—even, $E_n = \frac{\hbar^2\pi^2}{2ma^2}n^2$ [42]. For three dimensional case, set $\frac{-a}{2} < \delta_1^x, \delta_1^y, \delta_1^z < \frac{a}{2}$, $\varphi_n(\delta_1) = \sqrt{\frac{8}{a^3}}\cos\frac{n\pi}{a}\delta_1^x\cos\frac{n\pi}{a}\delta_1^y\cos\frac{n\pi}{a}\delta_1^z$, n— odd; $\varphi_n(\delta_1) = \sqrt{\frac{8}{a^3}}\sin\frac{n\pi}{a}\delta_1^x\sin\frac{n\pi}{a}\delta_1^y\sin\frac{n\pi}{a}\delta_1^z$,

n —even, for ground state where n=1, $\varphi_1\ (\ \delta_1) = \sqrt{\frac{8}{a^3}}\cos\frac{\pi}{a}\delta_1^x\cos\frac{\pi}{a}\delta_1^y\cos\frac{\pi}{a}\delta_1^z$.

Thus, the probability to find the particle in a space ($\frac{-a}{4} < \delta_2^x, \delta_2^y, \delta_2^z < \frac{a}{4}$) equals to:

$\iiint_{-a/4}^{a/4}\frac{8}{a^3}\cos^2\frac{\pi}{a}\delta_2^x\cos^2\frac{\pi}{a}\delta_2^y\cos^2\frac{\pi}{a}\delta_2^z d_{\delta_2^x} d_{\delta_2^y} d_{\delta_2^z} = 0.58.$

Therefore, a conclusion may be derived that it is reasonable to introduce $'\rho_n'$ (probability of finding particles with different $'\delta'$ distance between the center of the ion and the electrode surface) into the current density expression in quantum theory. The difficulty of predicting $'\rho_n'$ probably causes differences between the experimental results and simulation results in section 4.4.

CHAPTER 5

CONSLUSIONS AND RECOMMENDATIONS

The conclusions drawn from this research work are stated in Section 5.1. Recommendations for the future work are suggested in Section 5.2.

5.1 Conclusions

In this work, experimental investigation of process parameters in current efficiency using PECM has been performed. A simulation model has been proposed to further study the process. Based on the experiments and the simulation model the following conclusions can be drawn.

1. Screening design experiments showed that pulse electrochemical machining of nickel alloy was possible.
2. Electrolyte type and its flow rate influence current efficiency. With the application of sodium nitrate without citric acid and increase of its concentration, the current efficiency is higher when compared to the machining with citric acid. Faster electrolyte flow rate results in the high material removal rate, and hence the current efficiency is higher.
3. Current density also has an effect on the current efficiency. Current density increase causes better result of slowing down the electrical conductivity drop which is caused by predominant effect of gas generation. Thus, the current efficiency obtained may be higher.

4. The linear regression models for current efficiency were reliable by comparing the models developed with new experimental data.
5. The presented simulation model was able to predict the electrochemical machining process phenomena qualitatively correct. However, due to process complexity, the model's accuracy was insufficient. This could be caused by some assumptions that had to be taken into account to compromise simulation ability and computer memory. For example, one of the phenomena that have not been taken into account was the difficulty to describe process of electric double-layer formation on the workpiece surface that may affect current efficiency.

5.2 Recommendations for Future Work

1. The effects of group pulse and base time are recommended to study and in order to achieve high current efficiency and meet accuracy requirement at the same time.
2. The in-house built electrochemical cell needs to be designed with the need for controlling the electrolyte temperature and its flow rate more accurately.
3. In order to verify the general linear regression model, it is suggested to conduct further experiments with a wider range of parameter values. Interrelation terms, especially those with more than two-way factors, are recommended to consider.
4. Accounting for the effects of electric double-layer near the electrode will give a better simulation model in understanding of the performance characteristics.
5. Further work can be done on the current efficiency investigation of PECM process by applying quantum electrochemistry.

REFERENCES

[1] J.A. McGeough, Principles of Electrochemical Machining, Chapman and Hall, London, 1974

[2] H. El-hofy, Fundamentals of Machining Processes, Conventional and Nonconventional Processes, Taylor&Francis Group, 2007

[3] G.E. Benedict, Nontraditional Manufacturing Processes, Marcel Dekker, 1987

[4] K.P. Rajurkar, R.F. Ross, State-of-the-Art Assessment of the Pulsed Electrochemical Machining Process, *Report to the national Center for Manufacturing Sciences,* November 1991

[5] P. Guillermier, A. Blocquel, Process for Electrochemical Machining, US Patent 5516401 <http://www.patentstorm.us/patents/5516401/fulltext.html>

[6] Y. Mori, M. Shirakashi, Y. Toma, I. Kobata, T. Saito, Electrochemical Machining Method and Apparatus, US Patent 7255778, August 14, 2007

[7] B. Wei, J. Kozak, K.P. Rajurkar, Pulse Electrochemical Machining of Ti-6Al-4V Alloy, *Transaction of NAMR/SME,* Volume XXII, pp.141-147

[8] K.P. Rajurkar, D. Zhu, J.A. McGeough, J. Kozak, A.D. Silva, New Development in ElectroChemical Machining, *Annals of CIRP*, Vol.2, 1999, pp. 567-579

[9] J.A Kenney, G.S. Hwang, Electrochemical Machining with Ultrashort Voltage Pulses: Modeling of Charging Dynamics and Feature Profile Evolution, *Institute of physics publishing nanotechnology, Nanotechnology,* Vol. 16, 2005, pp.309-313

[10] J.A. McGeough (editor), Micromachining of Engineering Materials, Marcel Dekker, Inc. New York, 2002, pp.246-255

[11] M.A. Bejar, F. Gutierrez, On the Determination of Current Efficiency in Electrochemical Machining With a Variable Gap, *Journal of Materials Processing Technology (The Netherlands),*Vol. 37, No. 1-4, Feb. 1993 pp. 691-699

[12] P.R. Roberge, Corrosion Engineering: Principles and Practice, McGraw-Hill, 2008

[13] H.E. Townsend, Potential-pH Diagrams at Elevated Temperature for the System Fe-H_2O, *In Proceedings of the Fourth International Conference on Metallic Corrosion, NACE*, Houston, Corrosion Science, Vol. 10, 1970, pp.343-358

[14] CORWIKI^{TM}-The online corrosion encyclopedia, D.C. Silverman, Argentum Solutions, Inc, St. Louis, Missouri < http://www.argentumsolutions.com/>

[15] J. Bannard, Effect of Flow on the Dissolution Efficiency of Mild Steel during ECM, *Journal of Applied Electrochemistry*, Volume 7, 1977, pp.267-270

[16] K. Mao , D. Chin, Anodic Behavior of Mild Steel in $NaClO_3$ at High Current Densities, *Journal of Electrochemistry Society* , Volume 121, Issue 2, 1974, pp. 191-194

[17] J.P. Hoare , K. Mao, Anion Effects on the Dissolution of Steel in ECM Binary Electrolyte Systems, *Journal of Electrochemistry Society* ,Volume 120, Issue 11, 1973, pp. 1452-1456

[18] K. Mao, ECM Study in a Closed-Cell System, *Journal of the Electrochemical Society*, Volume 118, No. 11, 1971, pp.1870-1879

[19] K. Mao, M.A. LaBoda, J.P. Hoare, Anodic Film Studies on Steel in Nitrate-Based Electrolytes for Electrochemical Machining, *Journal of the Electrochemical Society*, Volume 119, No.4, 1972, pp.419-427

[20] E.J. Bergquist, L.J. Jennings, Electrolyte for Electrochemical Machining of Nickel base Superalloys, United States Patent 3975245 http://www.freepatentsonline.com/3975245.html

[21] M.A. Laboda, A.J. Chartrand, J.P. Hoare, R. Wiese, K. Mao, ECM of Nickel in $NaClO_3$ Solution, *Journal of the Electrochemical Society*, Volume 120, No. 5, 1973, pp.643-646

[22] K. Mao, Anodic Polarization Study of Mild Steel in NaCl Solution during Electrochemical Machining, *Journal of Electrochemistry Society,* Volume 120, Issue 8, 1973, pp. 1056-1060

[23] D. Chin, A.J. Wallance, Anodic Current Efficiency and Dimensional Control in Electrochemical Machining, *Journal of the Electrochemical Society*, Volume 120, No. 11, 1973, pp.1487-1493

[24] K.P. Rajurkar, D. Zhu, B. Wei, Minimization of Machining Allowance in Electrochemical Machining, *Annals of CIRP*, Volume 47, Issue 1, 1998, pp. 165-168

[25] J. Kozak, K.P. Rajurkar, B. Wei, Modeling and Analysis of Pulse Electrochemical Machining (PECM), *Transactions of the ASME,* Volume 116, 1994, pp.316-323

[26] S.A.K. Palmer, M.A. Breton, T.J. Nunno, D.M. Sullivan, N.F. Surprenant, Technical Resource Document: Treatment Technologies for Metal/Cyanide-Containing Wastes, Volume III, United States Environmental Protection Agency, 1988

[27] R.H. Shaw, Electrolyte for Electrochemically Machining Nickel Base Superalloys, US Patent 4026779, May 31, 1977

[28] ESPICorp Inc., <http://www.espi-metals.com/>
<http://www.espi-metals.com/tech/machiningnickel&alloys.pdf>

[29] S. Buljan, H. Lingertat, S.F. Wayne, Method of Machining Nickel based Superalloys, United States Patent 5216845, 1993

[30] M. Datta, L.T. Romankiw, D.R. Vigliotti, R.J. VonGutfeld, Jet and Laser-Jet Electrochemical Micromachining of Nickel and Steel, *Journal of Electrochemistry Society*, Volume 136, Issue 8, 1989, pp. 2251-2256

[31] K.P. Rajurkar, J. Kozak, B. Wei, Study of Pulse Electrochemical Machining Characteristics, *Annals of the CIRP*, Vol. 42, No. 1, 1993, pp. 231-234

[32] K.P. Rajurkar, B. Wei, J. Kozak, Modeling and Monitoring Interelectrode Gap in Pulse Electrochemical Machining, *Analysis of the CIRP*, Volume 44, pp.177-180

[33] M.H. Kutner, C.J. Nachtsheim, J. Neter, W. Li, Applied Linear Statistical Models, McGraw Hill Fifth edition, 2005

[34] J. Kozak, D. Gulbinowicz, Z. Gulbinowicz, The Mathematical Modeling and Computer Simulation of Pulse Electrochemical Micromachining, *Engineering Letter*, Volume16, pp.4-14

[35] A. James, An Introduction To Water Quality Modeling, Wiley-Interscience, 1984

[36] K.C.A. Smith, R.E. Alley, Electrical Circuits: An Introduction (Electronics Texts for Engineers and Scientists), Cambridge University Press, January 1992

[37] A.L. Shenkman, Circuit Analysis for Power Engineering Handbook, Springer First edition, February 1999

[38] P. Vanýsek, Electrochemical Series, Handbook of Chemistry and Physics, Chemical Rubber Company, 90th edition, 2009

[39] Chemical Engineering Module Model Library, COPYRIGHT 1994–2008 by COMSOL AB., <www.comsol.com>

[40] J.O'M. Bockris, Quantum Electrochemistry, Springer First edition, June 1979

[41] J.O'M. Bockris, A.K.N. Reddy, M.E. Gamboa-Aldeco, Modern Electrochemistry 2A: Fundamentals of Electronics (Hardcover), Springer Second edition, January 2001

[42] David Halliday, Fundamentals of Physics, Wiley 8th edition, 2007